

## Article

# Solar Potential in Saudi Arabia for Inclined Flat-Plate Surfaces of Constant Tilt Tracking the Sun

Ashraf Farahat <sup>1</sup>, Harry D. Kambezidis <sup>2,\*</sup> , Mansour Almazroui <sup>3,4</sup>  and Mohammed Al Otaibi <sup>5</sup>

<sup>1</sup> Department of Physics, College of General Studies, King Fahd University of Petroleum and Minerals, Dhahran SA-31261, Saudi Arabia; ashraf.farahat@kfupm.edu.sa

<sup>2</sup> Atmospheric Research Team, Institute of Environmental Research and Sustainable Development, National Observatory of Athens, GR-11810 Athens, Greece

<sup>3</sup> Centre of Excellence for Climate Change Research, Department of Meteorology, King Abdulaziz University, P.O. Box 80208, Jeddah SA-21589, Saudi Arabia; mansour@kau.edu.sa

<sup>4</sup> Climatic Research Unit, School of Environmental Sciences, University of East Anglia, Norwich NR4 7TJ, UK

<sup>5</sup> Health, Safety, Security and Environment Excellence Section, Industrial Security and Responsible Care Department, Sahara International Petrochemical Company, SIPCHEM, Jubail Industrial City 31961, Saudi Arabia; mood1408@hotmail.com

\* Correspondence: harry@noa.gr

**Abstract:** The objective of the present work is to investigate the optimally performing tilt angles in Saudi Arabia of solar panels that follow the daily motion of the Sun. To that end, the annual energy sums are estimated for surfaces with tilt angles in the range 5°–55° at 82 locations covering all Saudi Arabia. All calculations use a surface albedo of 0.2 and a near-real value, too. It is found that tilt angles of 40°, 45°, and 50°, respectively, are optimal for the three recently defined solar energy zones in Saudi Arabia. The variation of the energy sums in each energy zone on annual, seasonal and monthly basis is given for near-real ground albedos; the analysis provides regression equations for the energy sums as functions of time. A map of the annual global inclined solar energy for Saudi Arabia is derived and presented. The annual energy sums are found to vary between 2159 kWhm<sup>-2</sup>year<sup>-1</sup> and 4078 kWhm<sup>-2</sup>year<sup>-1</sup>. Finally, a correction factor, introduced in a recent publication, is used; it is confirmed that the relationship between the correction factor and either the tilt angle or the ground-albedo ratio has a general application and it may constitute a nomogram.

**Keywords:** solar potential; maximum energy; inclined surfaces; solar tracking; Saudi Arabia



**Citation:** Farahat, A.; Kambezidis, H.D.; Almazroui, M.; Al Otaibi, M. Solar Potential in Saudi Arabia for Inclined Flat-Plate Surfaces of Constant Tilt Tracking the Sun. *Appl. Sci.* **2021**, *11*, 7105. <https://doi.org/10.3390/app11157105>

Academic Editor: Alberto Benato

Received: 7 July 2021

Accepted: 28 July 2021

Published: 31 July 2021

**Publisher's Note:** MDPI stays neutral with regard to jurisdictional claims in published maps and institutional affiliations.



**Copyright:** © 2021 by the authors. Licensee MDPI, Basel, Switzerland. This article is an open access article distributed under the terms and conditions of the Creative Commons Attribution (CC BY) license (<https://creativecommons.org/licenses/by/4.0/>).

## 1. Introduction

Installations with tilted solar collectors for exploiting the renewable energy of the Sun have long been available in the market as commercial products. Solar flat-plate panels are nowadays widely used for converting solar energy into electricity (PV installations) or hot water (solar heating systems). These stationary systems consist of solar panels that receive solar radiation (i) at a fixed tilt angle with a southward orientation in the northern hemisphere or a northward orientation in the southern hemisphere; (ii) at a fixed tilt angle following the motion of the Sun; and (iii) at a varying tilt angle following the motion of the Sun, a mechanism that ensures that the solar rays always remain normal to the receiving plane. The mode (i) is widely used because of its lower cost for the static supporting frame of the solar system. The mode (ii), also known as a one- or single-axis system, provides higher solar energy on the inclined surface mounted on a vertical rotating axis, but has a slightly higher cost in order to maintain the moving parts. The mode (iii) is considered the most effective and is known as a two- or double-axis system. It provides the best performance of the solar systems rotating with the aid of a vertical and a horizontal axis, but is associated with higher maintenance costs because of more mechanical moving parts. The first category of solar systems is also called stationary or static, while the other two are dynamic, because of their Sun-tracking ability. Farahat et al. [1] examined the mode (i) for

the performance of flat-plate solar collectors in Saudi Arabia. This work is a continuation as it investigates the mode (ii) for the solar energy received on single-axis systems across the country.

Though static solar systems have received a lot of attention from researchers and solar energy developers, the dynamic ones (and especially the single-axis-mode collectors) have not been neglected either. Much effort has been invested at both the solar-energy-calculation level and the solar-system-development level to improve both the moving and the electronic parts for the Sun-tracking sensors [2,3]. The calculation of the optimum tilt angle and orientation for receiving maximum solar energy on solar flat-plate collectors has been the objective of various studies that use different strategies for obtaining solar radiation data: solar radiation modelling, e.g., [4,5]; combining with ground-based solar data, e.g., [6]; or utilising international data bases, e.g., [7,8]. Recently, a new method was presented by [9] for Greece and was applied in a recent study for Saudi Arabia [1]. The proposed method finds the maximum solar energy received by flat-plate collectors with southward (northward) orientation in the northern (southern) hemisphere. The idea behind this methodology is applied in the present study for solar collectors with constant tilt tracking the Sun.

An extensive review of the studies conducted for Saudi Arabia related to the present work can be found in [1].

From the above it is clear that no attempt has been made so far to construct a solar map for Saudi Arabia to show the solar potential on inclined flat planes that track the Sun. This gap is bridged in the present study, which includes three innovations. (i) For the first time, solar maps for Saudi Arabia showing maximum energy on optimally inclined flat surfaces tracking the Sun are derived. (ii) For the second time the three solar energy zones introduced by the same authors for Saudi Arabia [1] are also utilised here. (iii) The notion of the (ground-albedo) correction factor introduced in [1] is also used here, and the shape of the universal curves (representable as nomograms) of this parameter in relation to the tilt angle and the ground-albedo ratio is confirmed.

The structure of the paper is as follows. Section 2 describes the data collection and data analysis. Section 3 deploys the results of the study, while Section 4 presents the conclusions and main achievements of the work. Acknowledgements and References follow.

## 2. Materials and Methods

### 2.1. Data Collection

For the implementation of the study hourly values of the following parameters were collected: direct,  $H_b$  (in  $Wm^{-2}$ ), and diffuse,  $H_d$  (in  $Wm^{-2}$ ), horizontal solar radiation. These values were downloaded from the PV—Geographical Information System (PV-GIS) tool [10] using the latest Surface Solar Radiation Data Set—Heliostat (SARAH) 2005–2016 data base (12 years) [11,12]. The PV-GIS provides solar radiation data for any location in Europe, Africa, Middle East including Saudi Arabia, central and southeast Asia and most parts of the Americas. Solar radiation in the PV-GIS platform is calculated from satellite observations and modelling [13,14].

A set of 82 sites in Saudi Arabia was selected to cover the whole territory of the country. Hourly values of  $H_b$  and  $H_d$  were downloaded from PV-GIS for all 82 sites; Table 1 shows the names and provides the geographical coordinates of these sites, while Figure 1 is a map of Saudi Arabia showing their location. The criterion for selecting these sites is mentioned in [1].

**Table 1.** The 82 sites selected over Saudi Arabia to cover the whole territory of the country;  $\varphi$  is the geographical latitude, and  $\lambda$  the geographical longitude in the WGS84 geodetic system. This table is reproduction of Table 1 in [1].

#	Site	$\varphi$ (Degrees N)	$\lambda$ (Degrees E)
1	Dammam	26.42	50.09
2	Al Jubail	26.96	49.57
3	Ras Tanura	26.77	50.00
4	Abqaiq	25.92	49.67
5	Al Hofuf	25.38	49.59
6	Arar	30.96	41.06
7	Sakaka	29.88	40.10
8	Tabuk	28.38	36.57
9	Al Jawf	29.89	39.32
10	Riyadh	24.71	46.68
11	Al Qassim	26.21	43.48
12	Hafar Al Batin	28.38	45.96
13	Buraydah	26.36	43.98
14	Al Majma'ah	25.88	45.37
15	Hail	27.51	41.72
16	Jeddah	21.49	39.19
17	Jazan	16.89	42.57
18	Mecca	21.39	39.86
19	Medina	24.52	39.57
20	Taif	21.28	40.42
21	Yanbu	24.02	38.19
22	King Abdullah Economic City	22.45	39.13
23	Najran	17.57	44.23
24	Abha	18.25	42.51
25	Bisha	19.98	42.59
26	Al Sahmah	20.10	54.94
27	Thabhloten	19.83	53.90
28	Ardah	21.22	55.24
29	Shaybah	22.52	54.00
30	Al Kharkhir	18.87	51.13
31	Umm Al Melh	19.11	50.11
32	Ash Shalfa	21.87	49.71
33	Oroug Bani Maradh Wildlife	19.41	45.88
34	Wadi ad Dawasir	20.49	44.86
35	Al Badie Al Shamali	21.99	46.58
36	Howtat Bani Tamim	23.52	46.84
37	Al Duwadimi	24.50	44.39
38	Shaqra	25.23	45.24
39	Afif	24.02	42.95
40	New Muwayh	22.43	41.74
41	Mahd Al Thahab	23.49	40.85
42	Ar Rass	25.84	43.54
43	Uglat Asugour	25.85	42.15
44	Al Henakiyah	24.93	40.54
45	Ar Rawdah	26.81	41.68
46	Asbtar	26.96	40.28
47	Tayma	27.62	38.48
48	Al Khanafah Wildlife Sanctuary	28.81	38.92
49	Madain Saleh	26.92	38.04
50	Altubaiq Natural Reserve	29.51	37.23
51	Hazem Aljalamid	31.28	40.07
52	Turaif	31.68	38.69
53	Al Qurayyat	31.34	37.37
54	Harrat al Harrah Conservation	30.61	39.48
55	Al Uwayqilah	30.33	42.25
56	Rafha	29.63	43.49

Table 1. Cont.

#	Site	$\varphi$ (Degrees N)	$\lambda$ (Degrees E)
57	Khafji	28.41	48.50
58	Unnamed 1	21.92	51.99
59	Unnamed 2	21.03	51.16
60	Unnamed 3	22.33	52.53
61	Unnamed 4	23.42	50.73
62	Unnamed 5	21.28	48.03
63	Unnamed 6	31.70	39.26
64	Unnamed 7	32.02	39.65
65	Unnmaed 8	31.02	42.00
66	Unnamed 9	30.63	41.31
67	Unnamed 10	29.78	42.68
68	Unnamed 11	28.68	47.49
69	Unnamed 12	28.41	47.97
70	Unnamed 13	28.05	47.53
71	Unnamed 14	27.97	47.88
72	Unnamed 15	27.15	48.98
73	Unnamed 16	27.21	48.56
74	Unnamed 19	27.15	48.02
75	Unnamed 18	27.66	48.52
76	Unnamed 19	24.74	48.95
77	Unnamed 20	28.34	35.17
78	Unnamed 21	26.27	36.67
79	Unnamed 22	21.89	43.06
80	Unnamed 23	18.76	47.54
81	Unnamed 24	21.38	53.28
82	Unnamed 25	19.24	52.79

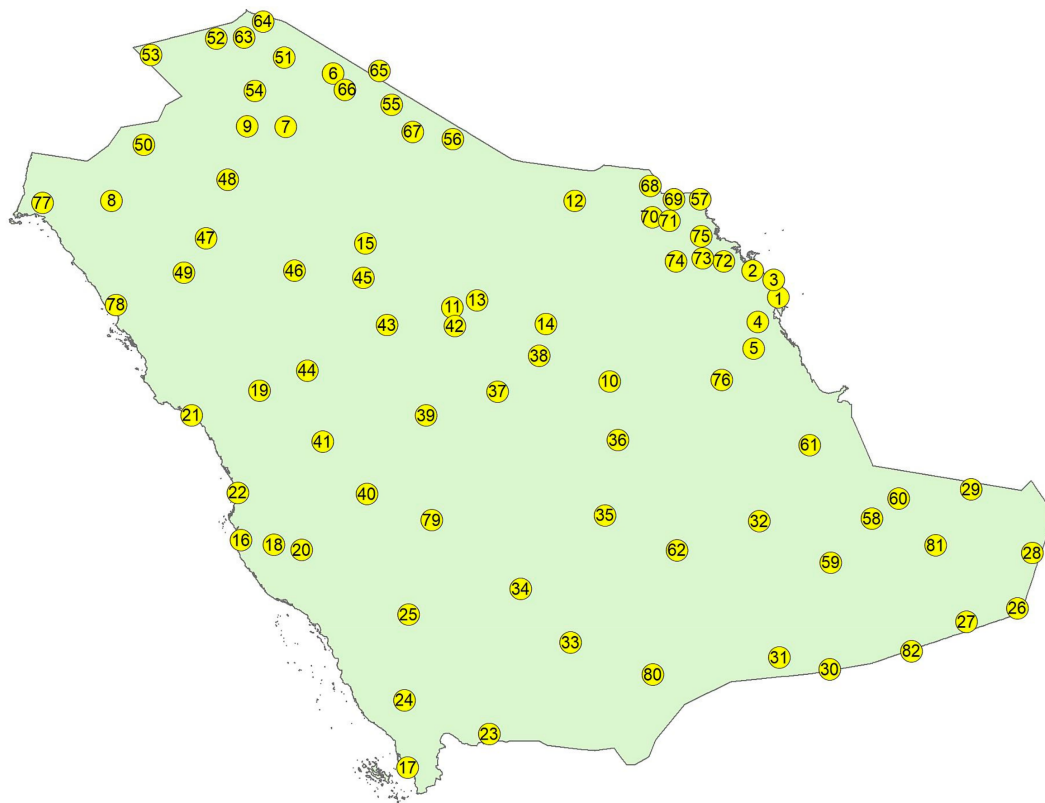


Figure 1. Distribution of the selected 82 locations in Saudi Arabia. The numbers in the circles refer to those in column 1 of Table 1. This figure is reproduction of Figure 1 in [1].

## 2.2. Data Processing and Analysis

This section consists of five steps, which are briefly described as more details can be found in the companion paper [1].

Step 1: The downloaded hourly data from the PV-GIS platform were converted from the universal time coordinate (UTC) into local standard time (LST = UTC + 3 h).

Step 2: The hourly global horizontal radiation,  $H_g$  (in  $Wm^{-2}$ ), values were estimated as the sum  $H_g = H_b + H_d$ .

Step 3: Use of the XRONOS.bas algorithm was made to calculate the solar altitudes,  $\gamma$ , for all sites in LST; this code is based on the SUNAE routine introduced by Walraven [15], and all subsequent modifications [16,17].

Step 4: All radiation and solar geometry values were assigned to the nearest LST hour (i.e., values at hh:mm LST were assigned to hh:00 LST).

Step 5: All hourly solar radiation values were retained for subsequent analysis that (i) were greater than  $0 Wm^{-2}$ , (ii) corresponded to  $\gamma \geq 5^\circ$ , and (iii)  $H_d \leq H_g$ .

For estimating global solar irradiance on an inclined plane fixed on a one-vertical axis tracker,  $H_{g,t,\beta}$  (in  $Wm^{-2}$ ), there was adopted the isotropic model of Liu-Jordan (L-J) [18] (the subscript t stands for 'tracking', and  $\beta$  is the tilt angle of the inclined plane with respect to the local horizon, in degrees). The isotropic model was used to estimate the ground-reflected radiation from the surrounding surface,  $H_{r,t,\beta}$  (in  $Wm^{-2}$ ), received on the inclined flat-plate surface. The L-J model has proved to be as efficient as other more sophisticated models in providing the tilted total solar radiation in many parts of the world [19]. For a Sun-tracking surface mounted on a vertical axis the received total solar radiation is given by a slight modification of Equation (1) in [1]

$$H_{g,t,\beta} = H_{b,t,\beta} + H_{d,t,\beta} + H_{r,t,\beta}, \quad (1)$$

where the subscript t denotes tracking by the inclined surface. According to Liu-Jordan [18]

$$H_{d,t,\beta} = H_d \cdot R_{di}, \quad (2)$$

$$H_{r,t,\beta} = H_g \cdot R_r \cdot \rho_{g0}, \text{ (or } \rho_g) \quad (3)$$

$$R_{di} = (1 + \cos\beta)/2, \quad (4)$$

$$R_r = (1 - \cos\beta)/2, \quad (5)$$

$$H_{b,t,\beta} = H_b \cdot \cos\theta / \sin\gamma, \quad (6)$$

$$\cos\theta = \sin\beta \cdot \cos\gamma \cdot \cos(\psi - \psi') + \cos\beta \cdot \sin\gamma. \quad (7)$$

where  $\theta$  is the incidence angle (the angle formed by the normal to the inclined surface and the line joining the surface with the centre of the Sun), and  $\psi, \psi'$  are the solar azimuths of the Sun and of the inclined plane, respectively;  $\psi = \psi'$  in this case. The parameters  $R_{di}$  and  $R_r$  are called the isotropic sky-configuration and ground-inclined plane-configuration factors, respectively. In the L-J model the ground albedo usually takes the value of  $\rho_{g0} = 0.2$  (Equation (3)), which is considered as reference in solar radiation modelling, although it refers to grassland areas [19]. Also, close-to-reality ground-albedo values,  $\rho_g$ , were used in this work. To retrieve such values for the 82 sites, use of the Giovanni portal [20] was made (details in [1]). Annual mean  $\rho_g$  values were then computed and used to re-calculate  $H_{g,t,\beta}$ .

The tilt angle in the present study varied in the range  $5^\circ$ – $55^\circ$  in increments of  $5^\circ$  (i.e., 11 tilt angles). This range fully covers all latitudes of Saudi Arabia (from  $\approx 18^\circ$  N to  $32^\circ$  N). For every site and tilt angle, hourly values of  $H_{g,t,\beta}$  were estimated from Equation (1) for both  $\rho_{g0} = 0.2$  and  $\rho_g$ . From the hourly  $H_{g,t,\beta}$  values, annual, seasonal and monthly solar energy sums (in  $kWhm^{-2}$ ) under all-sky conditions were estimated for 82 sites, 11 tilt angles, and 2 ground-albedo values.

### 3. Results

#### 3.1. Annual Energy Sumss

Annual solar energy sums were derived from the appropriate data base of each site for every tilt angle in the range  $5^{\circ}$ – $55^{\circ}$  (in  $5^{\circ}$  increments) by using both ground albedos,  $\rho_{g0}$  and  $\rho_g$  in Equations (1)–(7). From the calculated annual energy sums, the maximum sum and its corresponding (optimum) tilt angle were then obtained. Table 2 shows these maximum annual  $H_{g,t,opt. \beta}$  sums for all sites with the corresponding optimum tilts,  $opt. \beta$  (columns 2 and 3 for  $\rho_{g0}$  and  $\rho_g$ , respectively). From this table, it is seen that the average  $H_{g,t,opt. \beta} / \rho_{g0}$  (column 2) is  $2745.5 \text{ kWhm}^{-2}$ , while the average  $H_{g,t,opt. \beta} / \rho_g$  (column 3) is  $2769.7 \text{ kWhm}^{-2}$ , i.e., a 0.9% increase. Because of this small difference, the annual maximum solar energy sums from calculations with  $\rho_g$  were only considered in this study, as done in [1]. The reason for using both ground-albedo values was to show the difference in the derived maximum annual energy sums (columns 2, and 3 in Table 2). Therefore, it is interesting to see how the annual energy sums for the  $opt. \beta$ -derived values under the  $\rho_g$  calculations ( $H_{g,t,opt. \beta} / \rho_g$ ) are distributed across the 82 sites in Saudi Arabia. Figure 2 shows this spatial coverage of the country. Surprisingly no consistent pattern in terms of  $opt. \beta$  exists; to the contrary, there is a great mix of  $opt. \beta$  in the country, which does not seem to follow any particular logic. This may be attributed to intrinsic errors when deriving the solar horizontal radiation values in the PV-GIS tool. Therefore, such a distribution has no practical value to the solar energy industry as no clear application zones are formed as energy-application guidelines (as in the case of southward-oriented solar collectors in [1]) and may simply create confusion about the selection of the most appropriate tilt angle for the installation of a solar system at any particular location in Saudi Arabia. This unexpected outcome led to the idea of an ‘innocent manipulation’ of the  $opt. \beta$  values. This manipulation was based on the adoption of the three solar energy zones (SEZ) defined in [1]. This means that at a site for which the methodology has selected a ‘wrong’  $opt. \beta$ , a manual selection of the ‘correct’ tilt (according to the SEZ where the site itself belongs to) was made. Then, the corresponding annual solar energy sum was obtained. This is shown in the fourth column of Table 2, which provides the correct distribution of the 82 sites along the 3 SEZs (SEZ-A with selected  $opt. \beta = 40^{\circ}$ , SEZ-B with selected  $opt. \beta = 45^{\circ}$  and SEZ-C with selected  $opt. \beta = 50^{\circ}$ ). The corrected distribution is shown in Figure 3, which coincides with that of Figure 4 in [1]. After this correction, one would like to see what the created solar energy-sum differences are; Figure 4 shows these differences across all 82 sites. These energy differences,  $\Delta H_{g,t,\beta} / \rho_g$ , are defined as:  $\Delta H_{g,t,\beta} / \rho_g = H_{g,t,opt. \beta} / \rho_g - H_{g,t,selected opt. \beta} / \rho_g$ . From Figure 4a, it is seen that most of the sites 1–43 do not produce large differences, while the sites 44–82 result in annual energy deficits as low as  $-55 \text{ kWhm}^{-2}\text{year}^{-1}$ . The mean annual solar energy sums for all sites 1–43 and 44–82 are  $3026.3 \text{ kWhm}^{-2}\text{year}^{-1}$  and  $2954.7 \text{ kWhm}^{-2}\text{year}^{-1}$ , respectively, while their corresponding mean differences are  $-4.4 \text{ kWhm}^{-2}\text{year}^{-1}$  and  $-5.7 \text{ kWhm}^{-2}\text{year}^{-1}$ . This means that in the first group of sites, the absolute error derived from the manual selection of the optimum tilt angles is 0.15% ( $100 \times 4.4/3026.3$ ) while the error for the second group 0.19% ( $100 \times 5.7/2954.7$ ), both being quite insignificant. Therefore, the new distribution of the 82 sites in Figure 3 does not influence the solar energy yield across Saudi Arabia.

Contrary to the 3 SEZs adopted in the present work, Zell et al. [21] divided the country into five geographical areas in order to use and analyse the solar radiation data from [22]. Nevertheless, this division has of no practical value as it did not meet any solar radiation criteria.

Kaddoura et al. [7] estimated 12 optimal  $\beta$  for each of the 12 months of the year for Tabuk (#8 in Table 1), Al Jawf (#9), Riyadh (#10), Jeddah (#16), and Abha (#24). These  $\beta$  were derived from modelling and they, therefore, have a purely theoretical value.

In what follows, the notation  $H_{g,t,\beta} / \rho_g$  refers to the selected optimal  $\beta$ , i.e., to  $H_{g,t,selected opt. \beta} / \rho_g$ .

**Table 2.** Maximum  $H_{g,t,\beta}$  annual sums for the 82 sites in Saudi Arabia for optimal tilt angles, opt.  $\beta$ , with reference albedo  $\rho_{g0}$  and a near-real albedo  $\rho_g$ , under all-sky conditions for the period 2005–2016. The  $H_g$  values are rounded integers.

Site #	$H_{g,t,\beta/\rho_{g0}}$ (kWhm <sup>-2</sup> Year <sup>-1</sup> )/ Optimum $\beta$ (Degrees)	$H_{g,t,\beta/\rho_g}$ (kWhm <sup>-2</sup> Year <sup>-1</sup> )/ Optimum $\beta$ (Degrees)	$H_{g,t,\beta/\rho_g}$ (kWhm <sup>-2</sup> Year <sup>-1</sup> )/ Selected Optimum $\beta$ (Degrees)
1	2826/45	2846/45	2846/45
2	2824/45	2873/45	2873/45
3	2785/45	2782/40	2782/45
4	2862/40	2925/45	2925/45
5	2872/40	2925/45	2925/45
6	2921/45	2993/50	2993/50
7	3015/45	3081/50	3081/50
8	3149/45	3173/45	3173/45
9	2963/45	3022/50	3022/50
10	2937/45	2991/45	2991/45
11	2915/45	2955/45	2955/45
12	2748/45	2804/45	2804/45
13	2897/45	2944/45	2944/45
14	2900/45	2953/45	2953/45
15	2991/45	3035/45	3035/45
16	2912/40	2918/40	2917/40
17	2794/40	2767/35	2767/40
18	2903/40	2909/40	2909/40
19	3035/45	3021/40	3021/40
20	2926/40	2931/45	2931/40
21	3058/45	3054/45	3053/40
22	2946/40	2940/40	2940/40
23	3111/40	3129/45	3128/40
24	2803/40	2803/40	2803/40
25	3078/40	3086/40	3086/40
26	3041/40	3123/45	3109/40
27	3039/40	3118/45	3103/40
28	4013/50	4115/55	4078/45
29	2974/45	3043/45	3043/45
30	3268/45	3360/50	3314/40
31	3069/40	3144/45	3132/40
32	3002/40	3083/45	3069/40
33	3062/40	3144/45	3131/40
34	3017/40	3070/45	3062/40
35	2999/40	3061/45	3050/40
36	2984/40	3046/45	3046/45
37	2976/45	3028/45	3028/45
38	2899/45	2956/45	2956/45
39	3001/45	3032/45	3025/40
40	3065/45	3097/45	3091/40
41	3041/45	3038/45	3037/40
42	2917/45	2967/45	2967/45
43	3005/45	3033/45	3033/45
44	3078/45	3082/45	3076/40
45	2984/45	3008/45	3008/45
46	3073/45	3111/45	3111/45
47	3149/45	3239/50	3228/45
48	3004/45	3060/50	3058/45
49	3118/45	3183/50	3181/45
50	3027/45	3058/50	3056/45
51	2926/45	3004/50	3004/50
52	3666/55	3731/55	3692/50
53	2332/50	2365/50	2365/50
54	2936/45	2980/50	2980/50
55	2891/45	2964/50	2964/50
56	2272/50	2325/55	2324/50

Table 2. Cont.

Site #	$H_{g,t,\beta/\rho g0}$ (kWhm <sup>-2</sup> Year <sup>-1</sup> )/ Optimum $\beta$ (Degrees)	$H_{g,t,\beta/\rho g}$ (kWhm <sup>-2</sup> Year <sup>-1</sup> )/ Optimum $\beta$ (Degrees)	$H_{g,t,\beta/\rho g}$ (kWhm <sup>-2</sup> Year <sup>-1</sup> )/ Selected Optimum $\beta$ (Degrees)
57	2721/45	2700/40	2696/45
58	3018/40	3100/45	3100/45
59	3029/40	3111/45	3097/40
60	3011/40	3091/45	3091/45
61	2961/40	3042/45	3042/45
62	3015/40	3079/45	3069/40
63	2841/45	2892/50	2892/50
64	2877/45	2926/50	2926/50
65	2845/45	2913/50	2913/50
66	2852/45	2922/50	2922/50
67	2908/45	2978/50	2978/50
68	2546/55	2608/55	2553/45
69	2760/45	2827/50	2827/45
70	2763/40	2833/45	2833/45
71	2764/45	2821/45	2821/45
72	2779/40	2859/50	2859/45
73	2817/45	2863/45	2863/45
74	2995/45	3082/50	3067/45
75	2883/45	2947/50	2945/45
76	2113/50	2171/50	2159/45
77	2914/40	3002/50	3002/45
78	3145/45	3138/45	3125/40
79	3114/45	3086/45	3086/40
80	3041/40	3085/45	3078/40
81	3084/40	3170/45	3170/45
82	2988/45	3076/50	3051/40

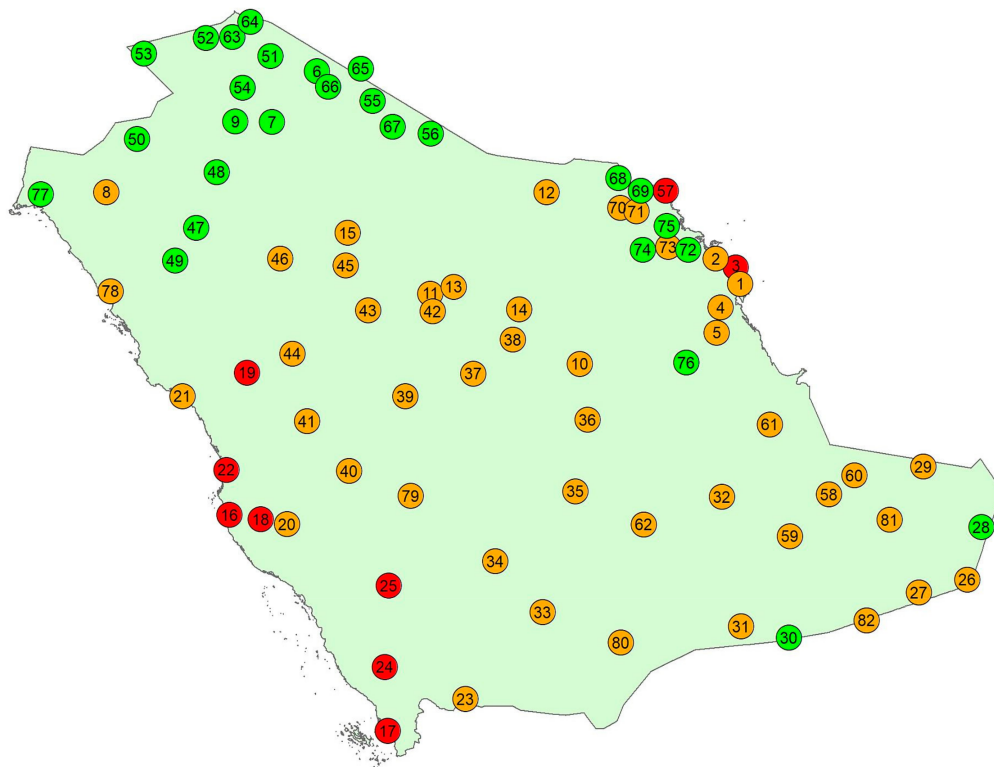
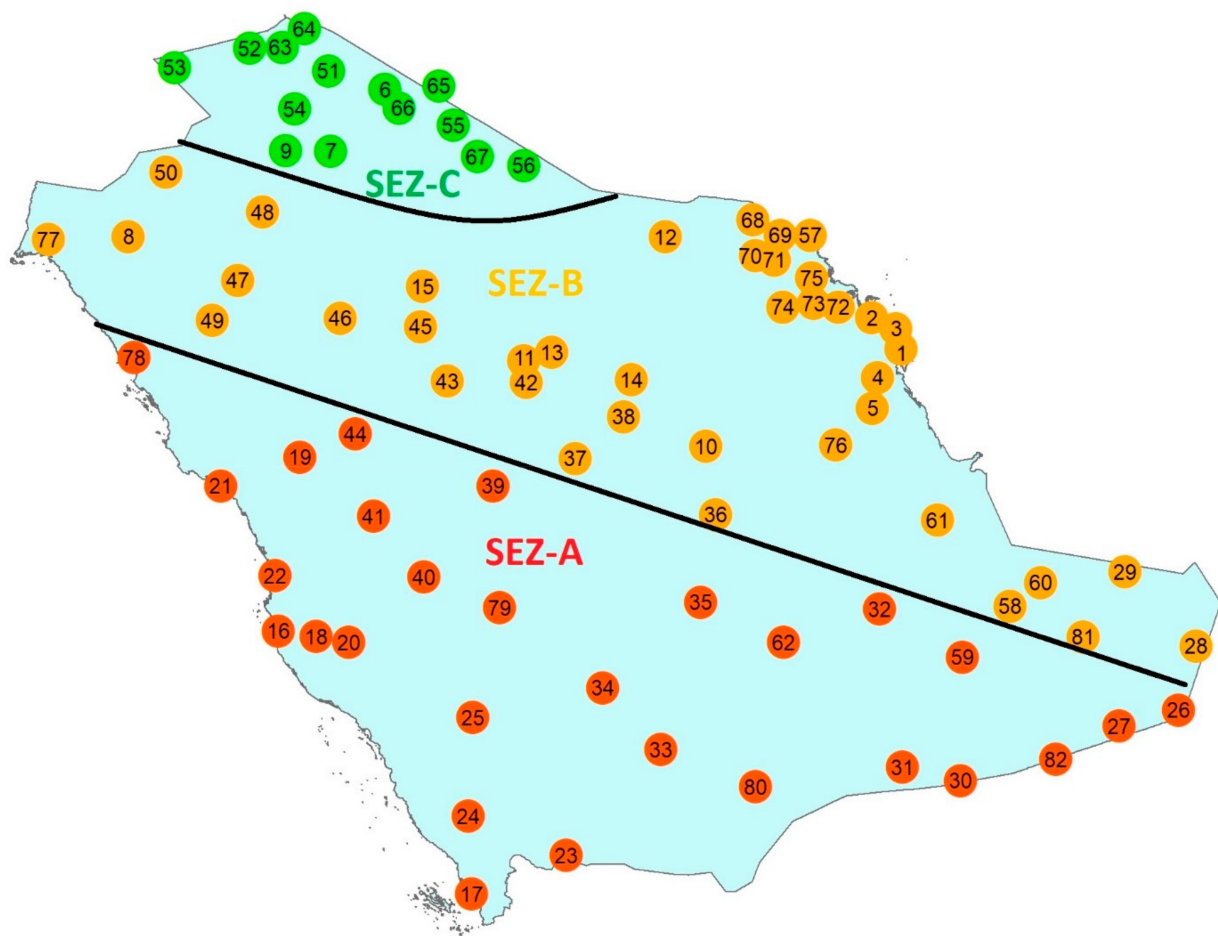


Figure 2. Distribution of the 82 selected sites in Saudi Arabia for maximum  $H_{g,t,opt. \beta/\rho g}$ . The numbers in the circles refer to those in column 1 of Table 1. The red circles correspond to sites with opt.  $\beta = 40^\circ$ , the orange with opt.  $\beta = 45^\circ$ , and the green ones with opt.  $\beta = 50^\circ$ .



**Figure 3.** Corrected distribution of the 82 selected sites in Saudi Arabia for maximum  $H_{g,t,opt. \beta/\rho_g}$ . The numbers in the circles refer to those in column 1 of Table 1. The red circles correspond to sites with selected opt.  $\beta = 40^\circ$  (SEZ-A), the orange with selected opt.  $\beta = 45^\circ$  (SEZ-B), and the green ones with selected opt.  $\beta = 50^\circ$  (SEZ-C). This figure is a reproduction of Figure 4 in [1].

### 3.2. Monthly Energy Sums

The intra-annual variation of  $H_{g,t,\beta/\rho_g}$  in each specific SEZ region is shown in Figure 5. Figure 5a refers to all sites in SEZ-A with optimal  $\beta = 40^\circ$ , Figure 5b to all sites in SEZ-B with optimal  $\beta = 45^\circ$ , Figure 5c to the sites in SEZ-C with optimal  $\beta = 50^\circ$ , and Figure 5d to all sites irrespective of SEZ and optimal  $\beta$ . The expressions for the lines that best fit the means and their coefficient of determination,  $R^2$ , are given in Table 3. It is seen that the  $R^2$  statistic obtains high values; this allows a solar energy user or investor in Saudi Arabia to estimate the monthly energy production in any of the three SEZs in an accurate way by applying the regression equations. The graphs also contain curves for the mean  $\pm 1$  standard deviation ( $\sigma$ ). It is apparent in all graphs (and especially in those that refer to SEZ-A and SEZ-B) that two secondary  $H_{g,t,\beta}$  maxima in March and October exist. These occur because of the variation of the solar elevation (or altitude,  $\gamma$ ) throughout the year at a certain time during the day. To demonstrate this, Figure 6 shows the variation of  $H_{g,t,40}$  during 2005–2016 at three sites in Saudi Arabia at high, mid and low latitudes, i.e., Arar (#6, 30.96 degN), Jeddah (#16, 21.49 degN), and Jazan (#17, 16.89 degN). Jazan has two energy maxima, one in April and another in October; Jeddah has two, one in March and another in October, while Arar shows a normal behaviour (maximum energy in July).

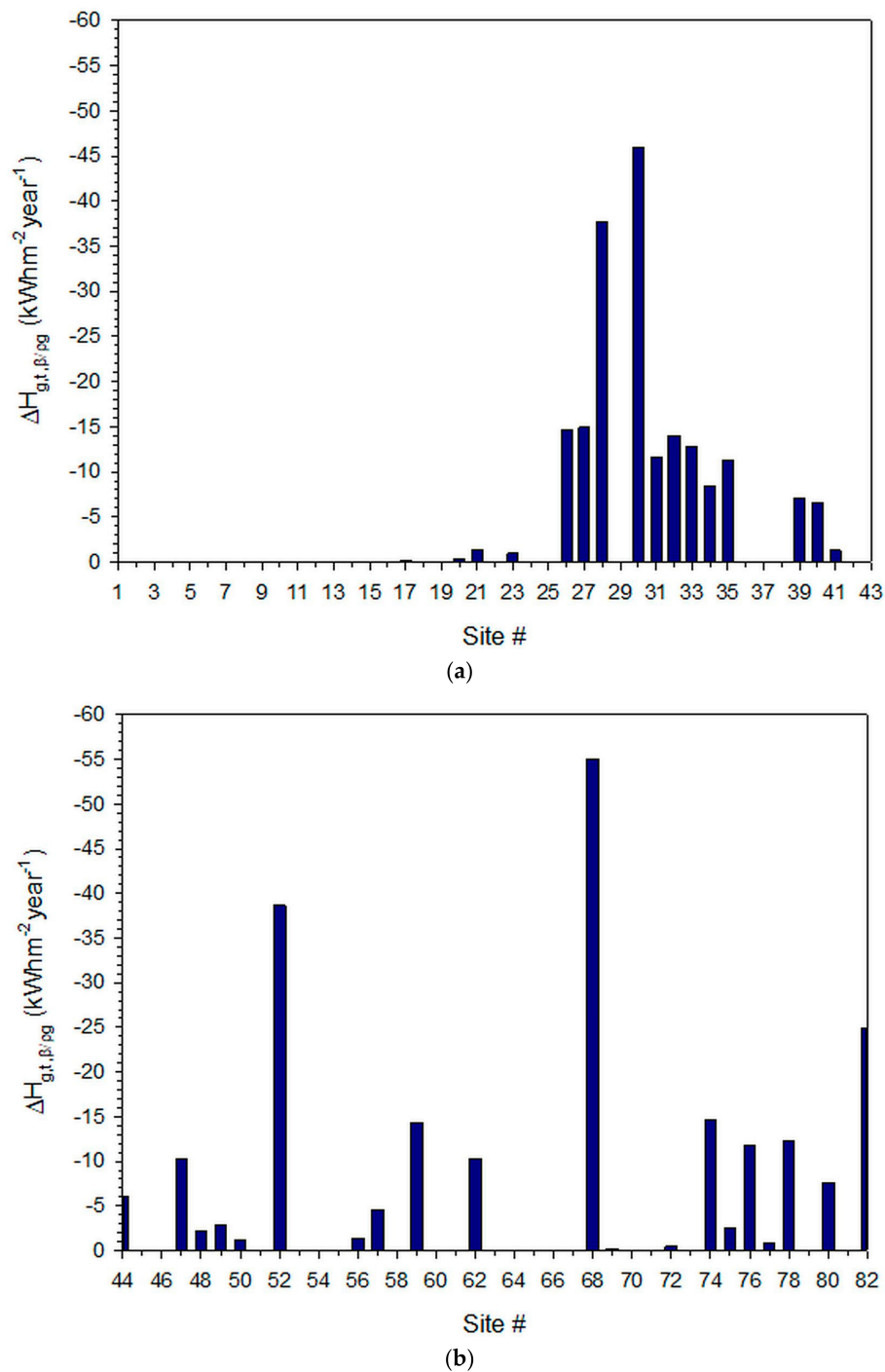
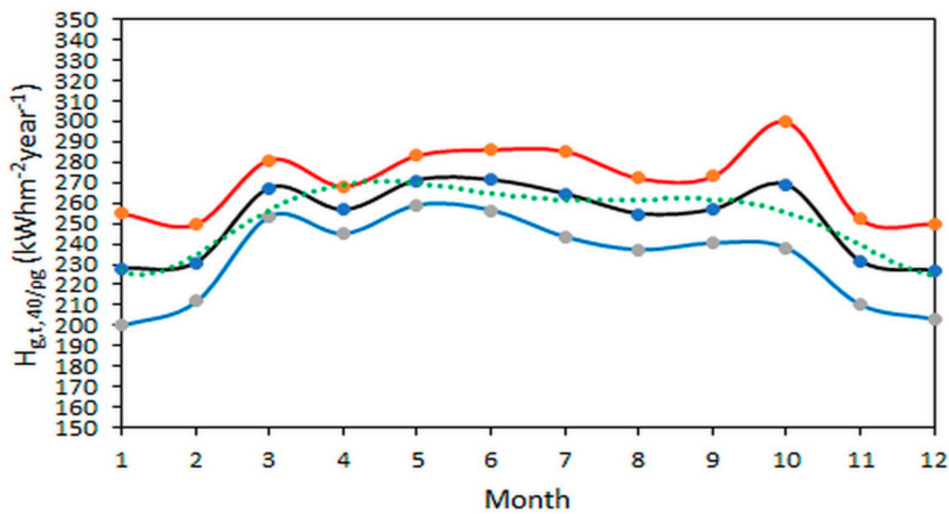


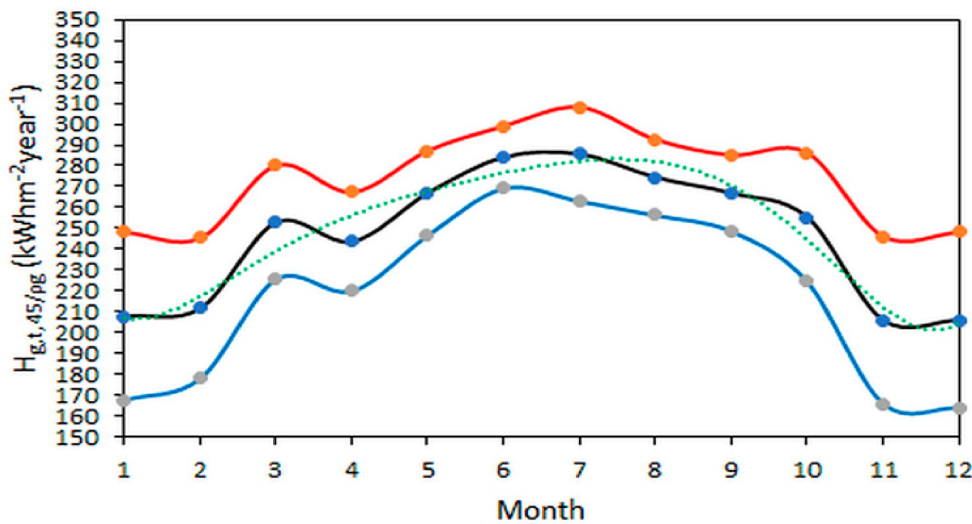
**Figure 4.** Differences of the annual maximum solar energy sums,  $\Delta H_{g,t,\beta/\rho g}$ , on flat planes between optimally-derived and selected tilt angles for sites (a) 1–43 and (b) 44–82, under all-sky conditions and averaged over the period 2005–2016.  $\Delta H_{g,t,\beta/\rho g} = H_{g,t,opt. \beta/\rho g} - H_{g,t,selected \ opt. \ \beta/\rho g}$ , where t refers to the tracking mode. The individual  $H_{g,t,\beta/\rho g}$  values in the differences are shown in Table 2 (columns 3 and 4, respectively) together with their optimal  $\beta$ .

**Table 3.** Regression equations for the best-fit curves to the monthly/seasonal mean  $H_{g,t,\beta/\rho g}$  sums averaged over all respective sites in the period 2005–2016, together with their  $R^2$  values;  $s$  is either month in the range 1–12 or season in the range 1–4 (1 = spring, 2 = summer, 3 = autumn, 4 = winter).

SEZ	Regression Equation	$R^2$
A (months)	$H_{g,t,40/\rho g} = 0.0054 s^6 - 0.218 s^5 + 3.4241 s^4 - 25.977 s^3 + 95.627 s^2 - 142.65 s + 296.38$	0.82
A (seasons)	$H_{g,t,40/\rho g} = -2.0956 s^3 - 0.5587 s^2 + 10.341 s + 787.81$	1
B (months)	$H_{g,t,45/\rho g} = 0.0049 s^6 - 0.1809 s^5 + 2.5754 s^4 - 18.215 s^3 + 65.134 s^2 - 90.585 s + 248.07$	0.94
B (seasons)	$H_{g,t,45/\rho g} = 44.915 s^3 - 367.88 s^2 + 870.06 s + 216.23$	1
C (months)	$H_{g,t,50/\rho g} = 0.051 s^6 - 0.1867 s^5 + 2.6857 s^4 - 19.7280 s^3 + 74.6630 s^2 - 106.5200 s + 235.9800$	0.98
C (seasons)	$H_{g,t,50/\rho g} = 74.807 s^3 - 627.99 s^2 + 1499.1 s - 174.91$	1
A,B,C (months)	$H_{g,t,\beta/\rho g} = 0.0051 s^6 - 0.1955 s^5 + 2.9007 s^4 - 21.259 s^3 + 77.717 s^2 - 112.08 s + 263.4$	0.94
A,B,C (seasons)	$H_{g,t,\beta/\rho g} = 33.967 s^3 - 286.87 s^2 + 683.91 s + 344.56$	1

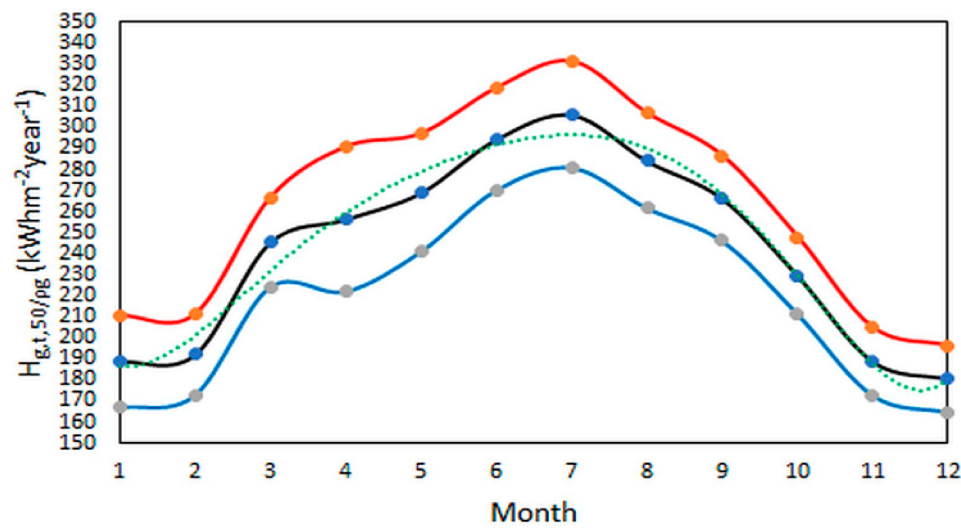


(a)

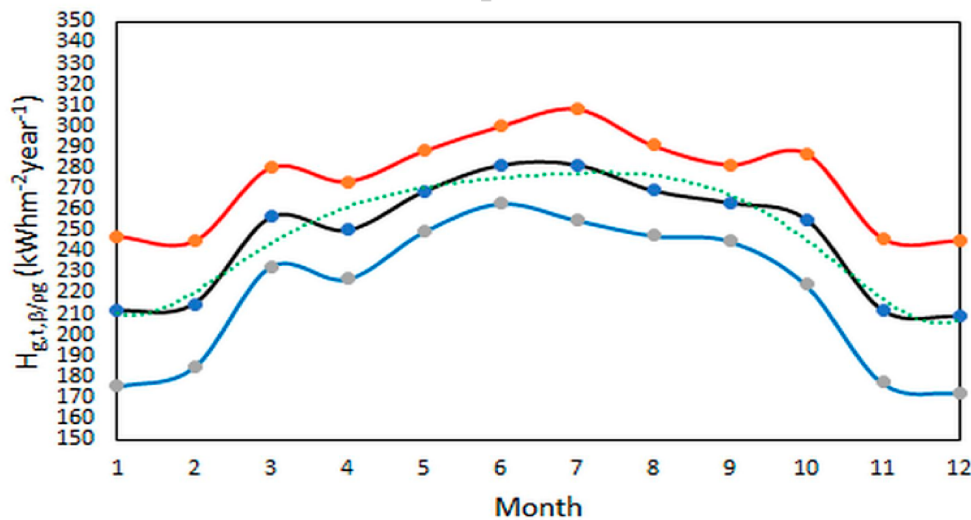


(b)

Figure 5. Cont.



(c)



(d)

**Figure 5.** Intra-annual variation of (a)  $H_{g,t,40/\rho_g}$  in SEZ-A, (b)  $H_{g,t,45/\rho_g}$  in SEZ-B, (c)  $H_{g,t,50/\rho_g}$  in SEZ-C, and (d)  $H_{g,t,\beta/\rho_g}$  in all SEZs, under all-sky conditions and averaged over the period 2005–2016. The black solid lines represent the monthly  $H_g$  sums averaged over all corresponding sites. The red lines correspond to the mean  $+1\sigma$  curves, and the blue lines to the mean  $-1\sigma$  curves. The green dotted lines refer to the best-fit curves to the mean ones.

### 3.3. Seasonal Energy Sums

In solar energy installations the minimum and maximum possible energy received by them corresponds to the winter and summer months, respectively. Therefore, this section is devoted to analysing the solar energy totals during all seasons, i.e., spring (March–April–May), summer (June–July–August), autumn (September–October–November), and winter (December–January–February).

Figure 7 presents the total solar energy received on a flat surface in SEZ-A (Figure 7a), SEZ-B (Figure 7b), SEZ-C (Figure 7c), and all SEZs (Figure 7d) under all-sky conditions during spring, summer, autumn, and winter. The energy values are sums for each season averaged over the period 2005–2016 and for all sites belonging to the same SEZ (or all SEZs). Table 3 gives the regression equations for the curves that best fit the mean ones in each case. It is interesting to observe that the fits are ideal ( $R^2 = 1$ ) in all cases.

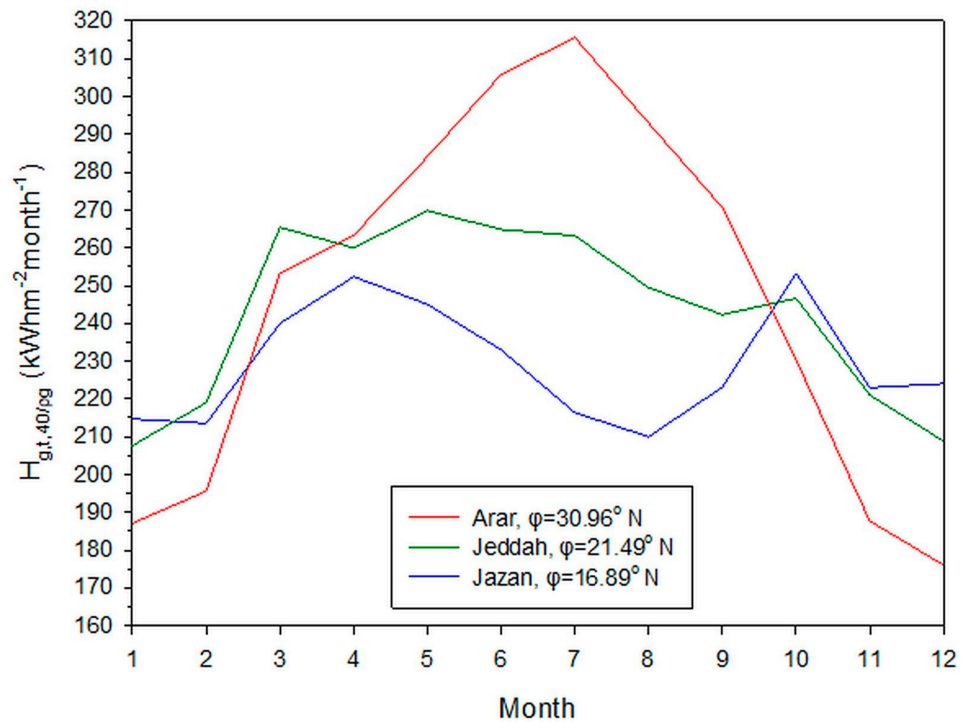


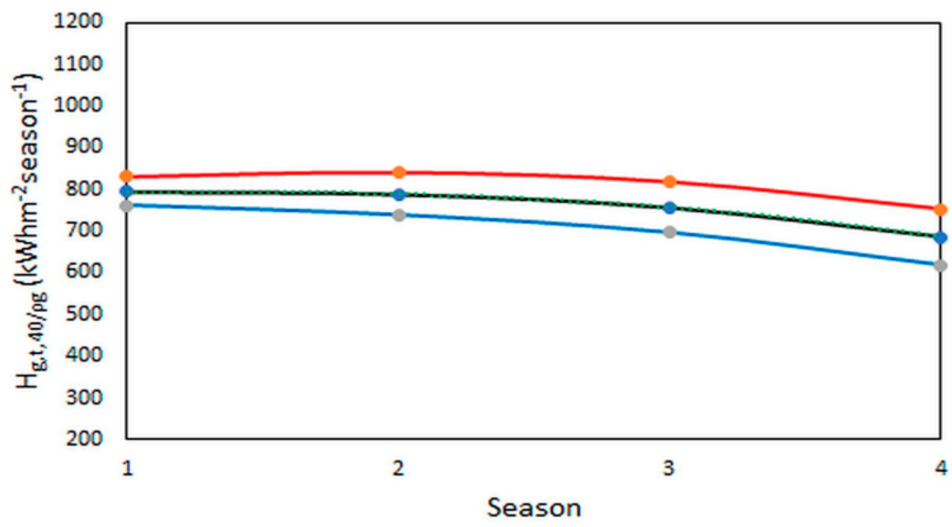
**Figure 6.** Intra-annual variation of the solar energy sum on a 40°-tilted plane,  $H_{g,t,40/\rho_g}$ , at the sites of Arar (#6 in Table 1), Jeddah (#16), and Jazan (#17). The values of  $H_{g,t,40/\rho_g}$  are averages over each month in the period 2005–2016 at 13.00 LST. The name and the geographical latitude of each site are shown in the legend.

### 3.4. Maps of Annual Energy Sums

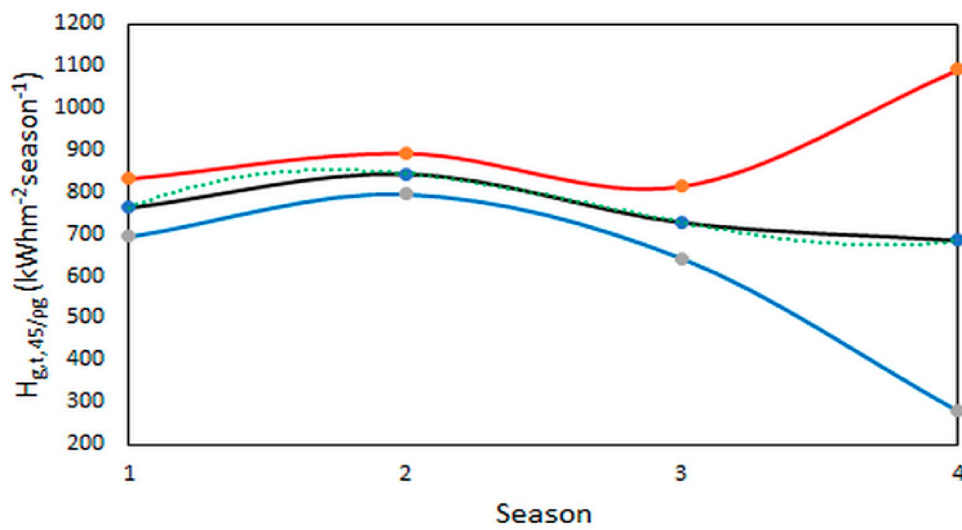
Figure 8 shows the solar potential over Saudi Arabia in terms of the annual  $H_g$  and  $H_{g,t,\beta/\rho_g}$  sums. A gradual increase in the annual solar potential in the direction NE–SW for both horizontal and optimally-inclined flat planes is observed. Very similar patterns to those in the present study are given in the Solar Radiation Atlas for Saudi Arabia [23]. Farahat et al. [1] have come to similar conclusion as regards the maximum solar energy received by flat-plate collectors oriented to south with optimum inclination. They justified this observation by the latitude gradient of the sites and the variability in meteorology across the country from north to south [24].

### 3.5. Evaluation of the PV-GIS Tool

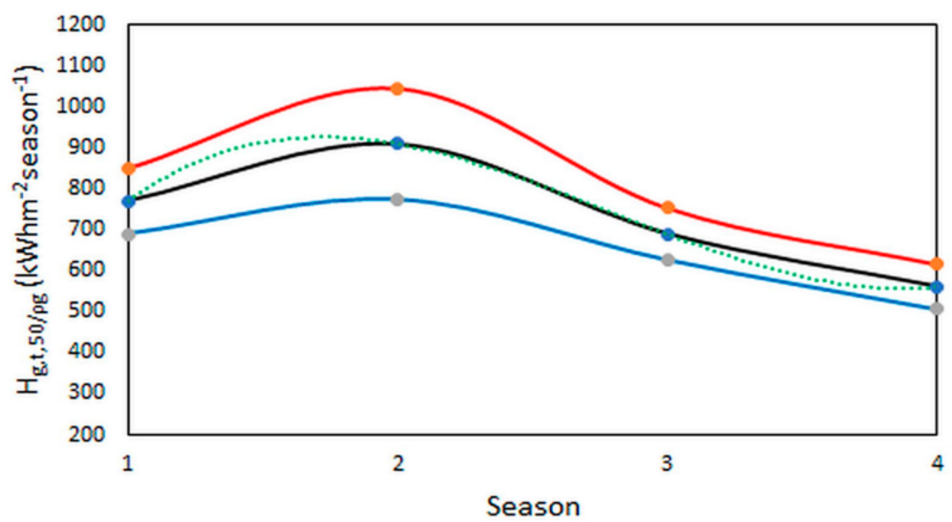
Various studies have presented validation results for the solar radiation PV-GIS-satellite-derived data by comparing them with ground-based solar radiation measurements from 30 BSRN (Baseline Solar radiation Network) stations [13,14,25]. The reported differences (%) in the form of  $100 \times (\text{estimated values} - \text{measurements}) / \text{measurements}$  were found to vary between  $-14\%$  and  $+11\%$  (the estimated values refer to the PV-GIS tool and the measurements come from the BSRN). Furthermore, Farahat et al. [1] demonstrated this comparison by taking monthly mean  $H_g$  values measured at the Actinometric Station of the National Observatory of Athens (ASNOA,  $37.97^\circ$  N,  $23.72^\circ$  E, 107 m above sea level) and corresponding values from the PV-GIS platform for the period 2005–2011. Figure 9 presents this comparison, which shows an excellent agreement ( $R^2 = 0.99$ ). Nevertheless, the PV-GIS-estimated values seem to overestimate the measured  $H_g$  ones by  $+10\%$ , a figure that is within the range in the above-mentioned studies, i.e., from  $-14\%$  to  $+11\%$ . Therefore, the PV-GIS data were accepted for use in the present study.



(a)



(b)



(c)

Figure 7. Cont.

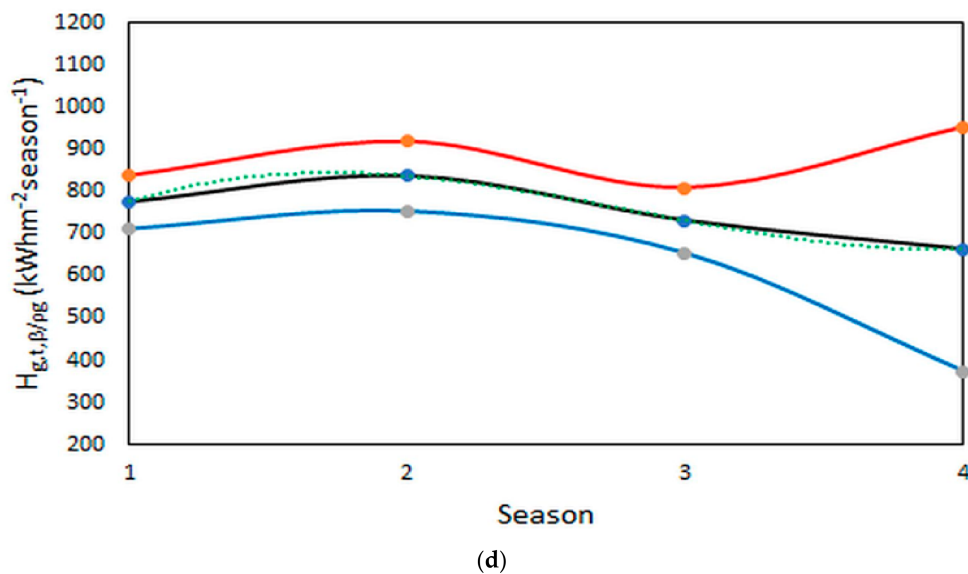


**Figure 7.** Seasonal variation of (a)  $H_{g,t,40}/\rho_g$  in SEZ-A, (b)  $H_{g,t,45}/\rho_g$  in SEZ-B, (c)  $H_{g,t,50}/\rho_g$  in SEZ-C, and (d)  $H_{g,t,\beta}/\rho_g$  in all SEZs. The black lines represent the seasonal mean. The red lines refer to the mean +  $1\sigma$  curves, and the blue ones to the mean −  $1\sigma$  curves, under all-sky conditions and averaged over the period 2005–2016. The green dotted lines refer to the best-fit curves to the mean ones. The numbers 1–4 in the  $x$ -axis refer to the seasons in the sequence spring to winter.

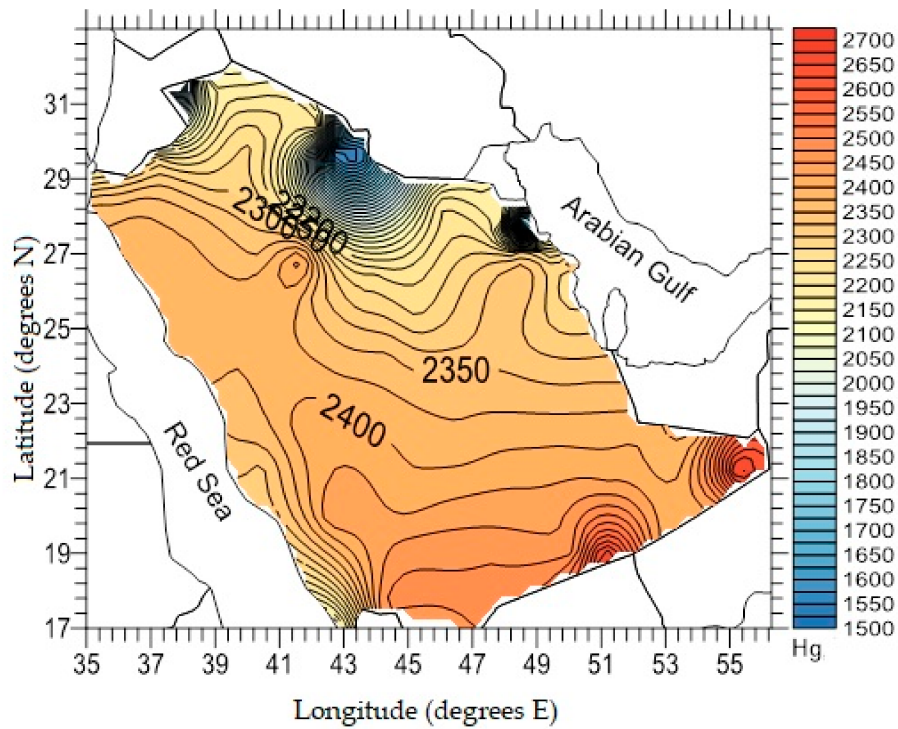
### 3.6. Correction Factor

Farahat et al. [1] introduced the notion of the correction factor, CF, which is defined as:  $CF = H_{g,t,\beta}/\rho_g / H_{g,t,\beta}/\rho_{g0}$ . Actually, CF is the ratio of the annual  $H_{g,t,\beta}$  sum at each site of the 82, calculated twice, once for  $\rho_{g0} = 0.2$  and a second time for  $\rho_g = \text{actual value}$ . The meaning of the CF is that it corrects the energy on an inclined surface under the influence of a ground albedo equal to 0.2 to that which is under the influence of the near-real ground-albedo value. Figure 10 presents the variation of CF as function of  $\beta$  for all 82 sites; the controlling parameter is the ratio  $\rho_r = \rho_g / \rho_{g0}$ . Note that the higher the  $\rho_r$  value is (i.e., for  $\rho_g > \rho_{g0}$ ), the more concave the best-fit curve is; in contrast, the lower the  $\rho_r$  value is (i.e., for  $\rho_g < \rho_{g0}$ ), the more convex the best-fit curve becomes. In the exceptional case of  $\rho_g = \rho_{g0}$  (as for site #24),  $CF = 1$ . All the data points at every  $\beta$  in Figure 10 correspond to the 82 sites. Figure 11 shows the distribution of the  $\rho_r$  values across the 82 sites.

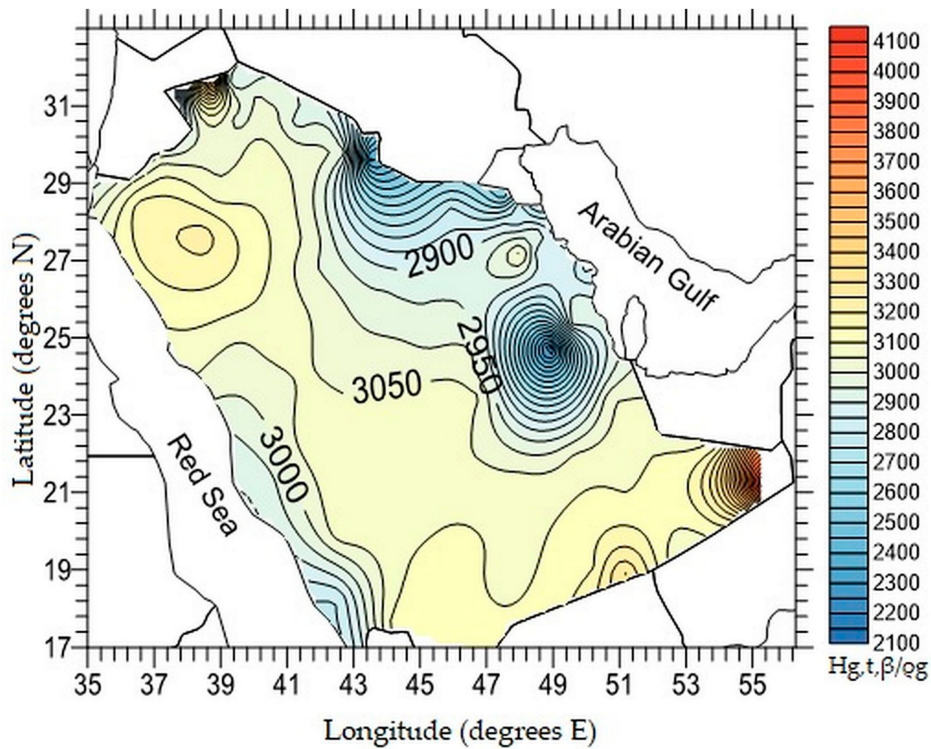
A diagram of CF vs.  $\rho_r$  is shown in Figure 12, where a linear relationship exists along all sites at the same  $\beta$ . The controlling parameter in this case is  $\beta$ ; as  $\beta$  increases, so does the slope of the linear fit to the data points. The data points along each line correspond to the 82 sites.

Beside the above, a more detailed analysis was performed for CF. In this analysis, the average values of  $CF = H_{g,t,\beta}/\rho_g / H_{g,t,\beta}/\rho_{g0}$  were calculated for all  $\beta$ s in the range  $5^\circ$ – $55^\circ$  and all sites belonging to the same SEZ, as well as all sites irrespective of SEZ. The results are shown in Figure 13. It is clearly seen that all mean CF values have an increasing trend with increasing  $\beta$ , because a flat-plate tilted surface receives more reflected radiation from its surroundings as its tilt angle increases. Moreover, the standard deviation,  $\sigma$ , of the mean CF increases with  $\beta$ , because  $H_{g,t,\beta}$  increases with increasing  $\beta$ , a fact that produces larger dispersion of the annual solar energy across all sites. In contrast,  $\sigma$  becomes smaller in the transition from SEZ-A to SEZ-C sites, a result that comes from the combination of the multitude of sites in each SEZ and the dispersion of the individual  $H_{g,t,\beta}$  values in the SEZ as shown by  $R^2$  in Table 3 (decreasing dispersion by increasing  $R^2$  from SEZ-A to SEZ-C). Note that the majority of the sites lies in SEZ-B (28 sites in SEZ-A, 40 in SEZ-B, and 14 in SEZ-C). Table 4 gives the regression equations for the curves that best fit the data points in each SEZ and all SEZs, too. These regression relationships have the same shape as those of the sites in Figure 10. This occurs because few sites have  $\rho_r < 1$ , and, therefore, the average

of the CF across all sites in the same SEZ, or all SEZs, gives a relationship resembling a site with  $\rho_r > 1$ .



(a)



(b)

**Figure 8.** Distribution of the annual (a)  $H_g$  ( $\text{kWhm}^{-2}\text{year}^{-1}$ ) and (b)  $H_{g,t,\beta/\rho_g}$  ( $\text{kWhm}^{-2}\text{year}^{-1}$ ) sums over Saudi Arabia, under all-sky conditions and averaged over the period 2005–2016. The different colouring in the  $H_g$  levels is due to the different colour scales used. Figure 8a is reproduction of Figure 7a in [1].

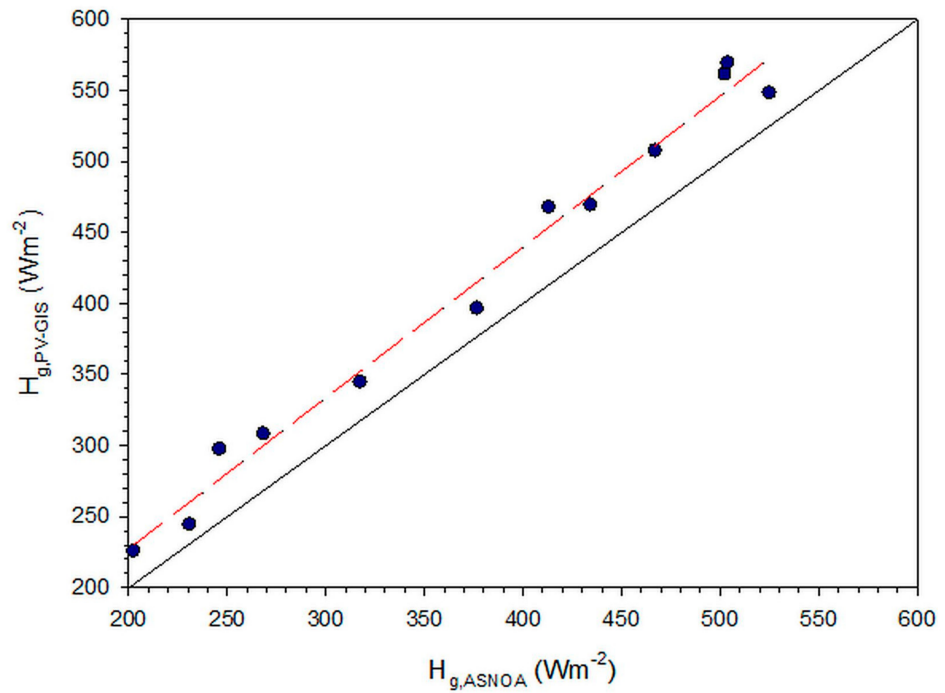


**Figure 9.** Comparison of monthly mean  $H_g$  values from PV-GIS to measured  $H_g$  values at ASNOA in the period 2005–2011. The red dashed line represents the best fit to the data points and is expressed by the regression equation:  $H_{g,PV-GIS} = 1.06 H_{g,ASNOA} + 14.96$  ( $R^2 = 0.99$ ). The solid black line is the 1:1 (or  $y = x$ ) line. This figure is reproduction of Figure 8 in [1].

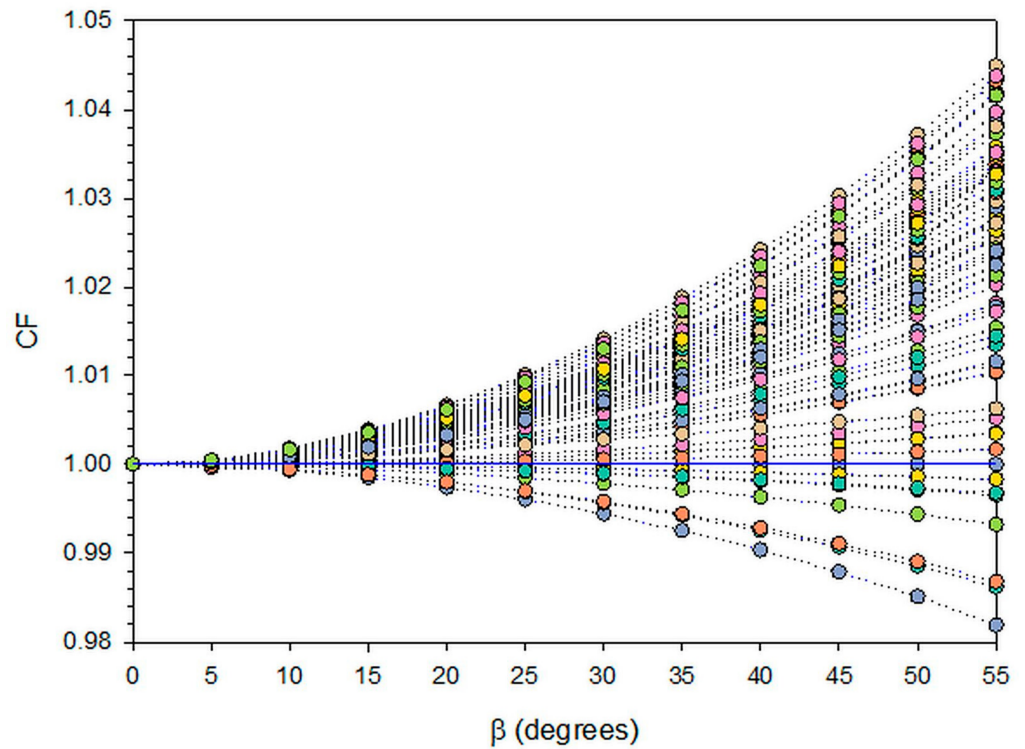
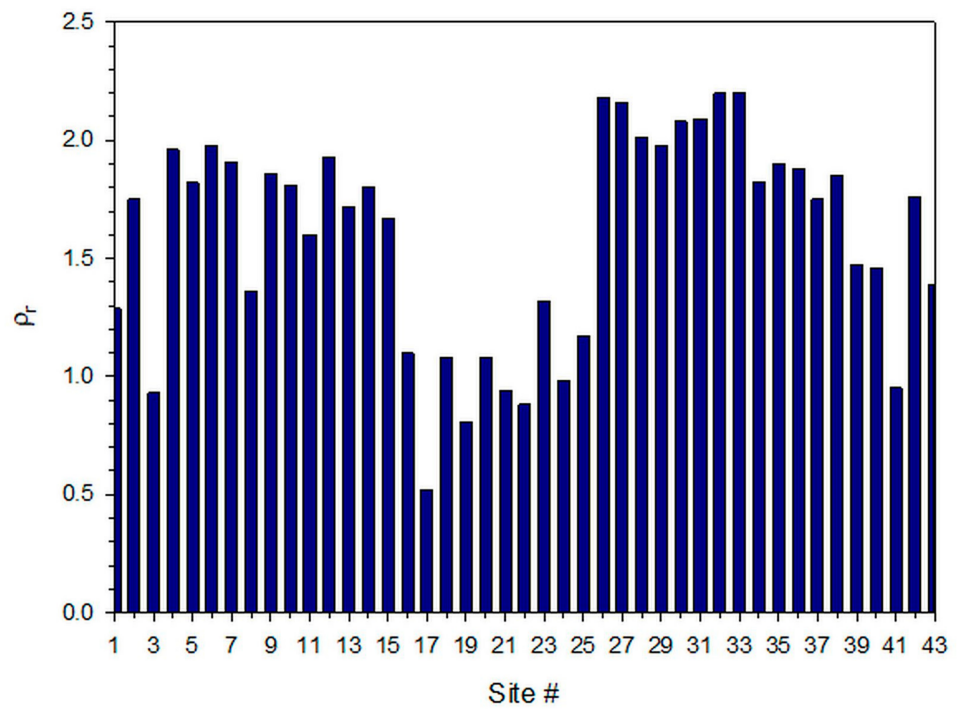
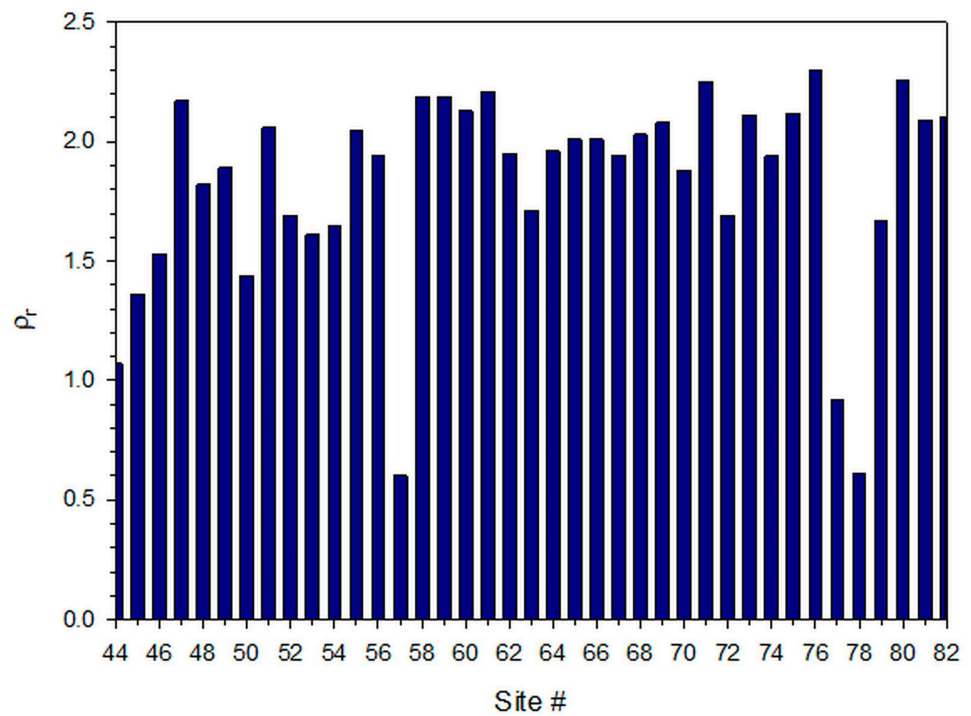


**Figure 10.** Variation of the correction factor, CF, as function of the tilt angle of the inclined flat plane,  $\beta$ , under all-sky conditions and averaged over the period 2005–2016. The dotted lines are the best-fit curves to the data points for each site, expressed as 3rd-order polynomials. The blue horizontal line indicates  $CF = 1$ .



(a)



(b)

**Figure 11.** Annual mean ratios of ground albedo,  $\rho_r$ , for the 82 sites in Saudi Arabia; (a) sites 1–43, (b) sites 44–82, averaged over the period 2005–2016. The site #24 has  $\rho_r = 1$ , because its  $\rho_g = \rho_{g0} = 0.2$ .

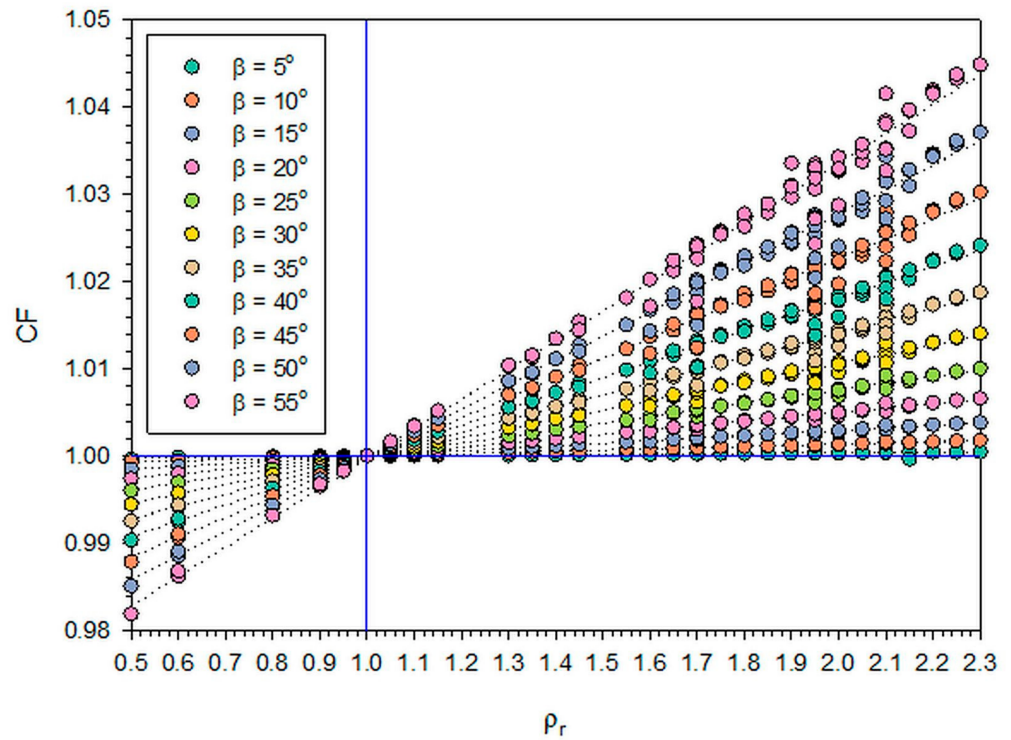


**Figure 12.** Variation of the correction factor, CF, as function of the ground-albedo ratio,  $\rho_r$ , for various tilt angles,  $\beta$ , for a flat plane tracking the Sun in Saudi Arabia, averaged over the period 2005–2016. The blue lines correspond to  $CF = \rho_r = 1$ . Notice that the datum point (1,1) is the site of Arar (#24), as expected. The black dotted lines are the best fits to the CFs of all sites having the same tilt angle.

**Table 4.** Regression equations for the best-fit curves to the CF– $\beta$  data points averaged over all respective sites in the period 2005–2016, together with their  $R^2$  values, for SEZ-A, SEZ-B, SEZ-C, and all SEZs.

$\beta$ (SEZ)	Regression Equation	$R^2$
40° (A)	$CF = 8.0863 \times 10^{-9} \beta^3 + 4.1615 \times 10^{-6} \beta^2 + 3.9379 \times 10^{-5} \beta + 0.9998$	1
45° (B)	$CF = 1.1413 \times 10^{-8} \beta^3 + 7.0911 \times 10^{-6} \beta^2 + 7.0532 \times 10^{-5} \beta + 0.9997$	1
50° (C)	$CF = 2.0347 \times 10^{-8} \beta^3 + 6.4319 \times 10^{-6} \beta^2 + 9.3106 \times 10^{-5} \beta + 0.9996$	1
40°, 45°, 50° (A,B,C)	$CF = 1.1802 \times 10^{-8} \beta^3 + 5.9782 \times 10^{-6} \beta^2 + 6.4260 \times 10^{-5} \beta + 0.9997$	1

From the above it is confirmed that the curves of CF vs.  $\beta$  (Figure 10) and CF vs.  $\rho_r$  (Figure 12) are universal and may be represented graphically as nomograms to allow any one of those variables to be calculated from the other two; this was demonstrated for the first time worldwide by [1].

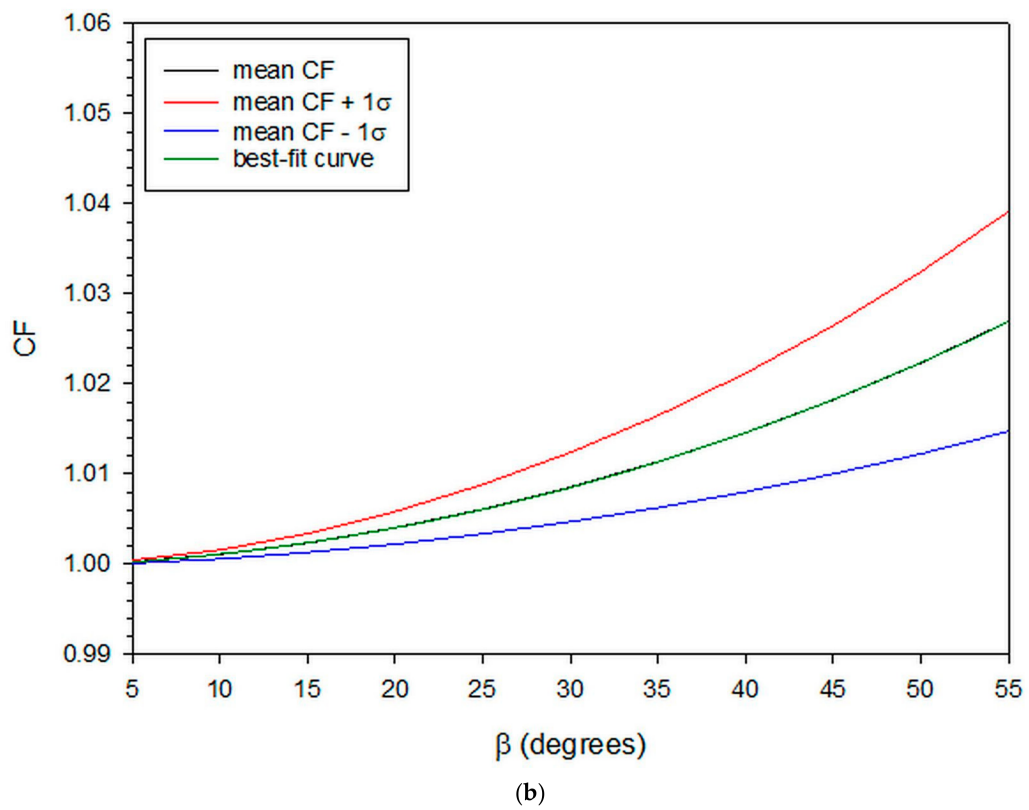
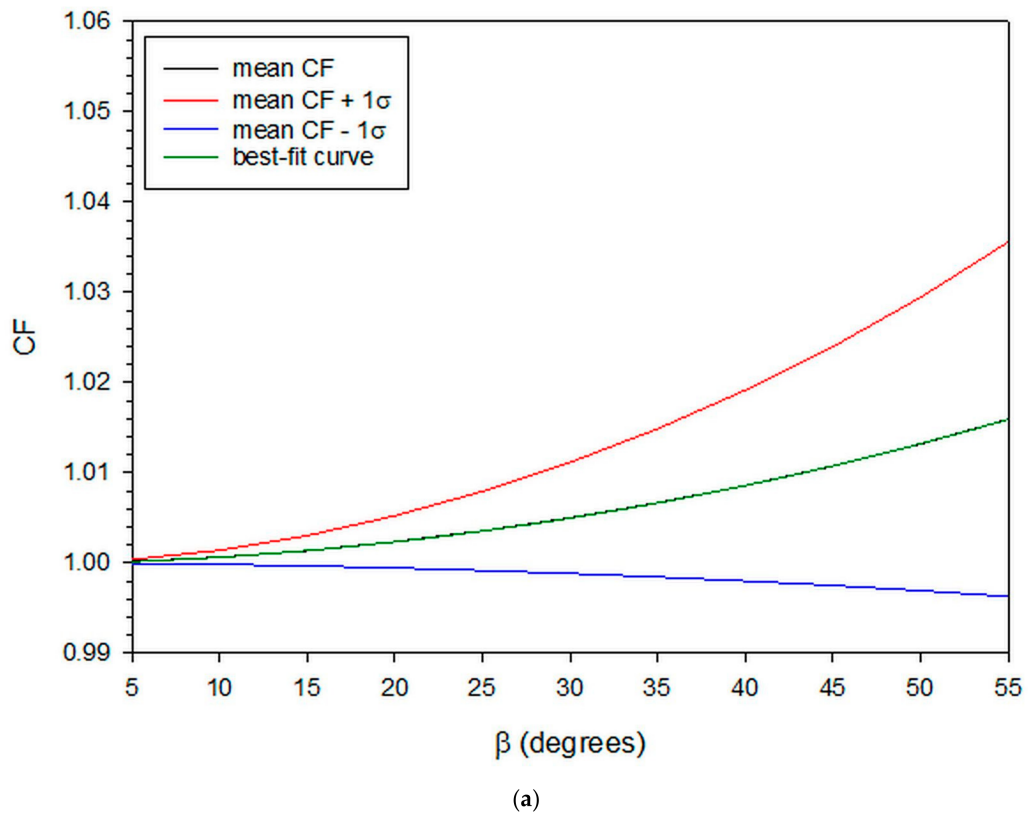
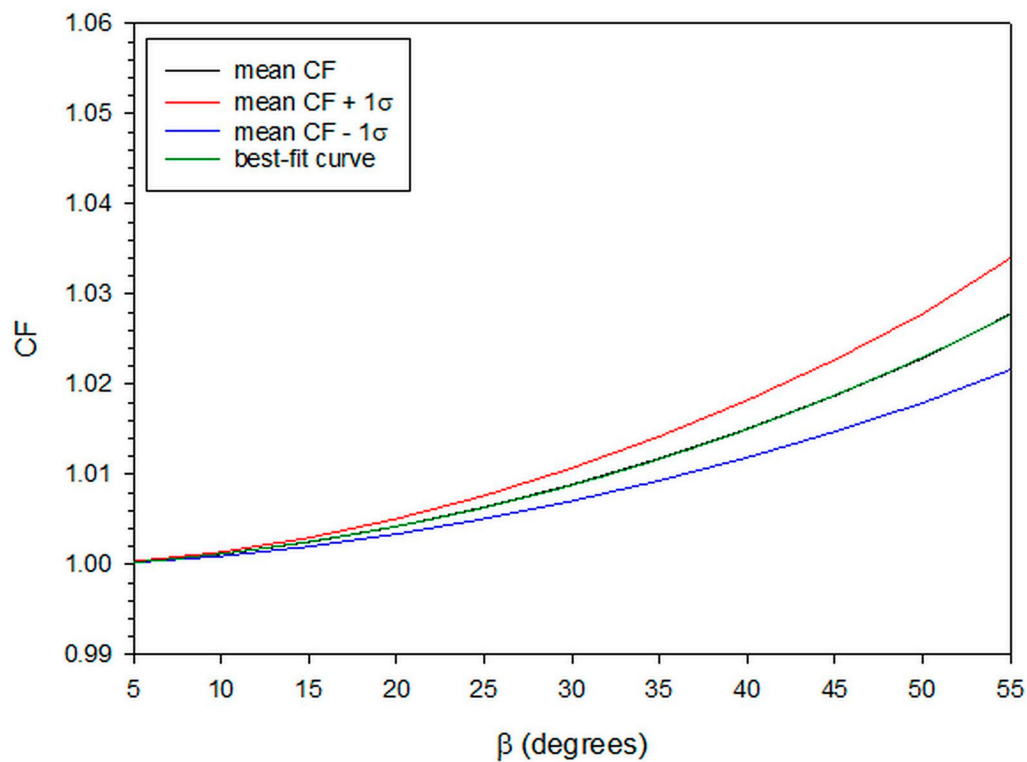
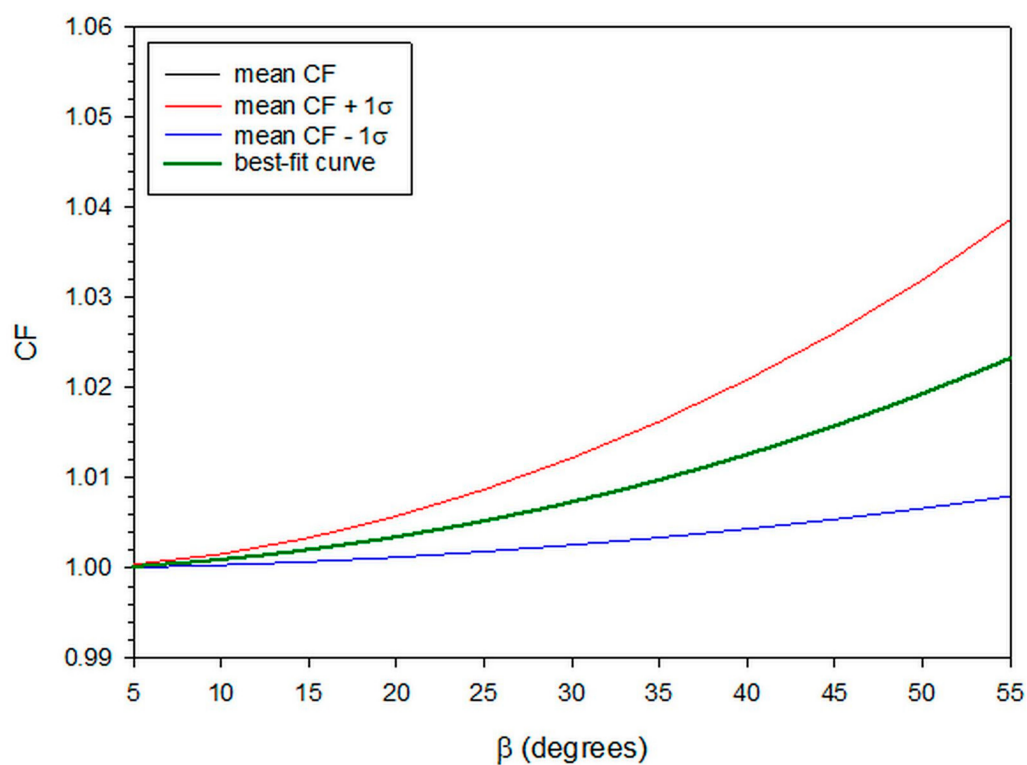


Figure 13. Cont.



(c)



(d)

**Figure 13.** Variation of the correction factor, CF, as function of the tilt angle,  $\beta$ , for an inclined surface in (a) SEZ-A, (b) SEZ-B, (c) SEZ-C, and (d) all SEZs, averaged over the period 2005–2016. The black solid lines are the mean CF values, while the red and blue ones correspond to the mean +  $1\sigma$ , and mean  $-1\sigma$ , respectively. The green dotted lines are the best fits to the mean curves and can hardly be distinguished as they coincide with the mean curves.

#### 4. Conclusions and Discussion

The present study investigated solar availability across Saudi Arabia on flat-plate solar panels that track the Sun along its daily path in the sky. The main objective was to find the optimum tilt angles of solar panels that produce maximum annual energy in this configuration under all-sky conditions. This was achieved by calculating the annual energy sum on flat-plate surfaces with tilt angles tracking the Sun in the range  $5^{\circ}$ – $55^{\circ}$  with an increment of  $5^{\circ}$  at 82 sites across Saudi Arabia; the solar availability on a horizontal plane was also included for reference purposes. The calculations of the energy received on the tilted surfaces were performed for a ground albedo equal to 0.2 (as a reference value) and also for a near-real ground albedo.

The first outcome of the work was that the optimum tilt angles for flat-plate solar collectors mounted on a vertical axis that track the Sun over Saudi Arabia are  $40^{\circ}$ ,  $45^{\circ}$ , and  $50^{\circ}$ . The second finding of the study was that these three optimum tilt angles can group the 82 sites into the three (solar energy) zones (SEZ) defined in [1], i.e., SEZ-A with  $40^{\circ}$ , SEZ-B with  $45^{\circ}$ , and SEZ-C with  $50^{\circ}$ . The third conclusion was related to the variation of the annual maximum solar energy in each SEZ, i.e., 2767–3314 kWhm<sup>-2</sup>year<sup>-1</sup> (average 3044.9 kWhm<sup>-2</sup>year<sup>-1</sup> in SEZ-A), 2159–4078 kWhm<sup>-2</sup>year<sup>-1</sup> (average 2975.6 kWhm<sup>-2</sup>year<sup>-1</sup> in SEZ-B), 2324–3692 kWhm<sup>-2</sup>year<sup>-1</sup> (average 2932.5 kWhm<sup>-2</sup>year<sup>-1</sup> in SEZ-C), and 2159–4078 kWhm<sup>-2</sup>year<sup>-1</sup> (average 2991.9 kWhm<sup>-2</sup>year<sup>-1</sup> in all SEZs). In relation to fixed-tilt solar systems reported in [1], the one-vertical axis solar systems in Saudi Arabia show an average increase in the maximum annual solar energy yield of +21.8% for SEZ-A, +22.6% for SEZ-B, +31.2% for SEZ-C, and +23.5% for all SEZs. Beside the annual energy sums, monthly solar energy values averaged over all locations belonging to the same SEZ as well as to all SEZs were estimated under all-sky conditions. Regression equations were provided as best-fit curves to the monthly mean energy sums that estimate the solar energy potential per SEZ (and all SEZs) with great accuracy ( $R^2 \geq 0.82$ ). These expressions may prove very useful to architects, civil engineers, solar energy engineers, and solar-energy-system investors in order to assess the solar energy availability in Saudi Arabia for Sun-tracking flat-plate solar collectors throughout the year.

Seasonal solar energy sums were also calculated. They were averaged over all sites in the same SEZ as well as over all sites (all SEZs), under all-sky conditions. For every case, regression curves that best fit the mean values were estimated with absolute accuracy ( $R^2 = 1$ ). Maximum sums were found in the summer (836.6 kWhm<sup>-2</sup>), and minimum ones in the winter (664.1 kWhm<sup>-2</sup>), as expected. The corresponding figures for the maximum energy received on a flat-plate solar collector in Saudi Arabia having an optimum tilt angle towards south are 659.9 kWhm<sup>-2</sup> and 532.3 kWhm<sup>-2</sup>, respectively for summer and winter [1]. Therefore, the single-axis solar systems provide a high increase in the maximum seasonal energy yield in comparison to the static ones of +26.8% and +24.8%, respectively.

The correction factor, CF, introduced in [1], was used in this work, too. A graph of CF as a function of the tilt angle (in the range  $5^{\circ}$ – $55^{\circ}$ ) showed exponential growth for sites having ratios  $\rho_r = \rho_g / \rho_0 > 1$ , or exponential decay in the cases of  $\rho_r < 1$ . Such curves are assumed to be universal (i.e., representable as nomograms), since similar graphs in [1] had the same shape. Nevertheless, this universality remains to be confirmed at other locations in the world with different climate and terrain characteristics. A graph of CF as a function of  $\rho_r$  was prepared for different values of the tilt angle in the range  $5^{\circ}$ – $55^{\circ}$ . Best-fit curves to the data points were estimated and were found to be linear, with decreasing slopes in proportion to decreasing tilt angles. These curves are also assumed to be nomograms, since similar graphs in [1] had the same shape. Nevertheless, this kind of nomogram has to be confirmed at other sites worldwide with different climate and terrain characteristics.

Three innovations appeared in the present study: (i) For the first time, solar maps for Saudi Arabia of the maximum energy received on optimally-inclined flat surfaces mounted on a system with a vertical axis that rotates and tracks the Sun were derived; (ii) for the first time, the three energy zones identified in [1] were used here and the same sites as

in [1] were accommodated in the same zones; (iii) universal curves (nomograms) of CF in relation to  $\beta$  and  $\rho_r$  were derived for this case, too.

As far as the utilisation of the results presented here is concerned, this can be summarised as follows. The solar industry has now a new rule for the inclined supporting frames mounted on single-axis solar systems; the inclined frame must have an angle of 40°, 45°, or 50° to the local horizon, depending on the SEZ to be installed. The same utilisation guidelines given by [1] for the static solar systems apply to this case, too.

This last paragraph of the work is devoted to the performance efficiency and operation cost of a static (fixed-tilt) and a single-axis solar PV system. Talavera et al. [26] examined the levelised cost of electricity (LCOE, in  $\text{€kWh}^{-1}$ ) for the two systems at five sites (two in Spain, one in Saudi Arabia, one in Brazil, and one in the USA) and found it varying according to site and type of the PV system. Overall, the LCOE for the single-axis PV system is a little bit higher than that for a fixed-tilt one. Nevertheless, the difference is not big and varies as +4.4%, 0%, 0%, +8.6%, and +1% for the five sites, respectively. Another study [27] concluded that the amount of electricity generation by a single-axis PV system in the USA is about 12–25% higher than that for a fixed-tilt one. A study for Jordan [28] showed that a dual-axis PV system generates 31.29% more annual electricity than a fixed-tilt one. For Europe, it has been found [29] that a single-axis PV system produces an annual energy yield of 30% higher in southern, and 25% in central Europe and up to 50% in northern Scandinavia.

**Author Contributions:** Data collection, data analysis, writing—review and editing, A.F.; Conceptualisation, methodology, data collection, data analysis, writing—original draft preparation, H.D.K.; writing—review and editing, M.A.; writing—review and editing, M.A.O. All authors have read and agreed to the published version of the manuscript.

**Funding:** Researchers would like to acknowledge the support provided by the Deanship of Scientific Research (DSR) at the King Fahd University of Petroleum and Minerals (KFUPM) for funding this work through project no. DF181010.

**Institutional Review Board Statement:** Not applicable.

**Informed Consent Statement:** Not applicable.

**Data Availability Statement:** The solar radiation data and the ground-albedo ones for Saudi Arabia are publicly available and were downloaded from the PV-GIS platform (<https://ec.europa.eu/jrc/en/pvgis> (accessed between 19 December 2020 and 16 January 2021)) and the Giovanni website (<https://giovanni.gsfc.nasa.gov/giovanni/> (accessed on between 6 and 30 May 2021)), respectively. The ASNOA solar radiation data are available on request, but they were used on a self-evident permission to the second author as ex. member and now Emeritus Researcher in the Institution.

**Acknowledgments:** The authors are thankful to the Giovanni-platform staff as well the MODIS-mission scientists and associated NASA personnel for the production of the ground-albedo data used in this research. They also thank the personnel of the PV-GIS platform for providing the necessary solar horizontal irradiances over Saudi Arabia. A.F. is thankful to Dalia Amer for her help in data organisation and processing. B.E. Psiloglou and N. Kappos are acknowledged for maintaining the solar radiation equipment on the ASNOA platform.

**Conflicts of Interest:** The authors declare no conflict of interest.

## References

1. Farahat, A.; Kambezidis, H.D.; Almazroui, M.; Ramadan, E. Solar Potential in Saudi Arabia for Southward-Inclined Flat-Plate Surfaces. *Appl. Sci.* **2021**, *11*, 4101. [[CrossRef](#)]
2. Akbar, H.S. Design of Sun Tracker System for Solar Energy Applications. *J. Phys. Res.* **2015**, *1*, 29–34.
3. Hafez, A.Z.; Yousef, A.M.; Harag, N.M. Solar Tracking Systems: Technologies and Trackers Drive Types—A Review. *Renew. Sustain. Energy Rev.* **2018**, *91*, 754–782. [[CrossRef](#)]
4. Altarawneh, I.S.; Rawadieh, S.I.; Tarawneh, M.S.; Alrowwad, S.M.; Rimawi, F. Optimal Tilt Angle Trajectory for Maximizing Solar Energy Potential in Ma'an Area in Jordan. *J. Renew. Sustain. Energy* **2016**, *8*, 033701. [[CrossRef](#)]
5. Evseev, E.G.; Kudish, A.I. The Assessment of Different Models to Predict the Global Solar Radiation on a Surface Tilted to the South. *Sol. Energy* **2009**, *83*, 377–388. [[CrossRef](#)]

6. Kambezidis, H.D. The Solar Radiation Climate of Athens: Variations and Tendencies in the Period 1992–2017, the Brightening Era. *Sol. Energy* **2018**, *173*, 328–347. [CrossRef]
7. Kaddoura, T.O.; Ramli, M.A.M.; Al-Turki, Y.A. On the Estimation of the Optimum Tilt Angle of PV Panel in Saudi Arabia. *Renew. Sustain. Energy Rev.* **2016**, *65*, 626–634. [CrossRef]
8. Ohtake, H.; Uno, F.; Oozeki, T.; Yamada, Y.; Takenaka, H.; Nakajima, T.Y. Estimation of Satellite-Derived Regional Photovoltaic Power Generation Using a Satellite-Estimated Solar Radiation Data. *Energy Sci. Eng.* **2018**, *6*, 570–583. [CrossRef]
9. Kambezidis, H.D.; Psiloglou, B.E. Estimation of the Optimum Energy Received by Solar Energy Flat-Plate Convertors in Greece Using Typical Meteorological Years. Part I: South-Oriented Tilt Angles. *Appl. Sci.* **2021**, *11*, 1547. [CrossRef]
10. Huld, T.; Müller, R.; Gambardella, A. A New Solar Radiation Database for Estimating PV Performance in Europe and Africa. *Sol. Energy* **2012**, *86*, 1803–1815. [CrossRef]
11. Urraca, R.; Gracia-Amillo, A.M.; Koubli, E.; Huld, T.; Trentmann, J.; Riihelä, A.; Lindfors, A.V.; Palmer, D.; Gottschalg, R.; Antonanzas-Torres, F. Extensive Validation of CM SAF Surface Radiation Products over Europe. *Remote Sens. Environ.* **2017**, *199*, 171–186. [CrossRef]
12. Urraca, R.; Huld, T.; Gracia-Amillo, A.; Martinez-de-Pison, F.J.; Kaspar, F.; Sanz-Garcia, A. Evaluation of Global Horizontal Irradiance Estimates from ERA5 and COSMO-REA6 Reanalyses Using Ground and Satellite-Based Data. *Sol. Energy* **2018**, *164*, 339–354. [CrossRef]
13. Mueller, R.W.; Matsoukas, C.; Gratzki, A.; Behr, H.D.; Hollmann, R. The CM-SAF Operational Scheme for the Satellite Based Retrieval of Solar Surface Irradiance—A LUT Based Eigenvector Hybrid Approach. *Remote Sens. Environ.* **2009**, *113*, 1012–1024. [CrossRef]
14. Amillo, A.G.; Huld, T.; Müller, R. A New Database of Global and Direct Solar Radiation Using the Eastern Meteosat Satellite, Models and Validation. *Remote Sens.* **2014**, *6*, 8165–8189. [CrossRef]
15. Walraven, R. Calculating the Position of the Sun. *Sol. Energy* **1978**, *20*, 393–397. [CrossRef]
16. Wilkinson, B.J. An Improved FORTRAN Program for the Rapid Calculation of the Solar Position. *Sol. Energy* **1981**, *27*, 67–68. [CrossRef]
17. Kambezidis, H.D.; Papanikolaou, N.S. Solar Position and Atmospheric Refraction. *Sol. Energy* **1990**, *44*, 143–144. [CrossRef]
18. Liu, B.; Jordan, R.C. The Long-Term Average Performance of Flat-Plate Solar-Energy Collectors. *Sol. Energy* **1963**, *7*, 53–74. [CrossRef]
19. Kambezidis, H.D.; Psiloglou, B.E.; Gueymard, C. Measurements and Models for Total Solar Irradiance on Inclined Surface in Athens, Greece. *Sol. Energy* **1994**, *53*, 177–185. [CrossRef]
20. Acker, J.G.; Leptoukh, G. Online Analysis Enhances Use of NASA Earth Science Data. *Eos Trans. Am. Geophys. Union* **2007**, *88*, 14. [CrossRef]
21. Zell, E.; Gasim, S.; Wilcox, S.; Katamoura, S.; Stoffel, T.; Shibli, H.; Engel-Cox, J.; Al Subie, M. Assessment of Solar Radiation Resources in Saudi Arabia. *Sol. Energy* **2015**, *119*, 422–438. [CrossRef]
22. ESMAR. Global Solar Atlas 2.0. 2019. Available online: <https://globalsolaratlas.info/map?c=11.523088,8.613281,3> (accessed on 1 July 2021).
23. National Renewable Energy Laboratory. Kingdom of Saudi Arabia: Solar Radiation Atlas. Available online: <https://digital.library.unt.edu/ark:/67531/metadc690351/> (accessed on 1 July 2021).
24. Marey, H.S.; Gille, J.C.; El-Askary, H.M.; Shalaby, E.A.; El-Raey, M.E. Aerosol Climatology over Nile Delta Based on MODIS, MISR and OMI Satellite Data. *Atmos. Chem. Phys.* **2011**, *11*, 10637–10648. [CrossRef]
25. Mueller, R.; Behrendt, T.; Hammer, A.; Kemper, A. A New Algorithm for the Satellite-Based Retrieval of Solar Surface Irradiance in Spectral Bands. *Remote Sens.* **2012**, *4*, 622–647. [CrossRef]
26. Talavera, D.L.; Muñoz-Cerón, E.; Ferrer-Rodríguez, J.P.; Pérez-Higueras, P.J. Assessment of Cost-Competitiveness and Profitability of Fixed and Tracking Photovoltaic Systems: The Case of Five Specific Sites. *Renew. Energy* **2019**, *134*, 902–913. [CrossRef]
27. Drury, E.; Lopez, A.; Denholm, P.; Margolis, R. Relative Performance of Tracking versus Fixed Tilt Photovoltaic Systems in the USA. *Prog. Photovolt. Res. Appl.* **2013**, *22*, 1302–1315. [CrossRef]
28. Hammad, B.; Al-Sardeah, A.; Al-Abed, M.; Nijmeh, S.; Al-Ghandoor, A. Performance and Economic Comparison of Fixed and Tracking Photovoltaic Systems in Jordan. *Renew. Sustain. Energy Rev.* **2017**, *80*, 827–839. [CrossRef]
29. Huld, T.; Cebecauer, T.; Šúri, M.; Dunlop, E.D. Analysis of One-Axis Tracking Strategies for PV Systems in Europe. *Prog. Photovolt. Res. Appl.* **2010**, *18*, 183–194. [CrossRef]